UNIVERSITAT DE BARCELONA

Final Degree Project

Biomedical Engineernig Degree

“ Pipeline development for realistic synthetic database generation of SPECT neuroimaging “

Barcelona, 11th June 2025

Author: Sara Álvarez Gamero

Director/s: Aida Niñerola, Raúl Tudela

Tutor: Raúl Tudela

Abstract

This Final Degree Project introduces a simulation pipeline for generating realistic brain SPECT images using Monte Carlo methods. Built on real anatomical MRI and CT data from patients with diagnosed or suspected Parkinson's disease, the pipeline creates synthetic images by first generating activity and attenuation maps that replicate radiotracer distribution and tissue densities. These are then used as inputs for the SimSET simulation engine to produce synthetic SPECT projections.

A core feature of the pipeline is its iterative framework. Simulated reconstructions are compared to real clinical SPECT images using anatomical atlases to quantify regional differences. These discrepancies inform successive updates to the activity map, gradually refining image realism across iterations. The approach enables the generation of synthetic SPECT studies that closely resemble real data, while maintaining known ground truth—key for evaluating and validating quantification methods in nuclear medicine.

The pipeline is modular, reproducible, and scalable, with integrated quality controls and standardized preprocessing steps. It lays the groundwork for creating a database of synthetic realistic neuroimaging studies. The project contributes to the advancement of validation for quantification imaging tools, particularly for Parkinson's disease research and clinical validation.

Keywords

SPECT, Parkinson's disease, Simulation, Monte Carlo, Quantification, DaTscan, reconstruction

Abstract

Aquest Treball de Final de Grau presenta un pipeline de simulació per generar imatges cerebrals de SPECT realistes mitjançant mètodes de Monte Carlo. Utilitza dades anatòmiques reals d'RM i TC de pacients amb diagnòstic o sospita de malaltia de Parkinson per construir mapes d'activitat i atenuació que simulen la distribució del radiotraçador i les densitats tissulars. Aquests mapes són emprats com a entrada per al simulador SimSET, que genera projeccions sintètiques de SPECT.

Un dels elements clau del projecte és el seu enfocament iteratiu. Les reconstruccions simulades es comparen amb les imatges clíniques utilitzant atlas anatòmics per detectar diferències regionals. Aquestes discrepàncies es fan servir per actualitzar progressivament el mapa d'activitat, millorant iterativament el realisme de les imatges. El resultat són estudis sintètics de SPECT molt similars als reals, però amb veritat de base coneguda, essencial per validar mètodes de quantificació en medicina nuclear.

El pipeline és modular, escalable i incorpora mecanismes de control de qualitat i preprocesament estandarditzat. Representa una base sòlida per al desenvolupament d'una base de dades sintètica realista d'estudis neurofuncionals. El projecte contribueix a l'avanç de les eines de validació per mètodes de quantificació d'imatge, especialment en l'àmbit de la malaltia de Parkinson.

Paraules clau

SPECT, Malaltia de Parkinson, Simulació, Monte Carlo, Quantificació, DaTscan, Reconstrucció

Acknowledgements

The completion of this project has not been easy, but I have always felt supported by those who accompanied me throughout the process. For that reason, I want to express my deepest gratitude in this section.

First and foremost, I would like to thank Raúl Tudela and Aida Niñerola, who have guided and mentored me over the past months. Their patience and constant willingness to help have been invaluable, especially during moments when I felt stuck or frustrated.

I am also sincerely grateful to my family, who have always encouraged me to keep going and believed in me, even during the most challenging times.

Finally, I would like to thank everyone who has shared this journey with me, especially my friends from university, with whom I have shared mutual support as we each worked through our respective projects.

List of Figures

List of Tables

List of Abbreviations

PD: Parkinson's Disease

SNpc: substantia nigra pars compacta

PET: Positron Emission Tomography

SPECT: Single Photon Emission Computed Tomography

DAT: DaTscan, Dopamine Transporter

SUR: Specific Uptake Ratio

MRI: Magnetic resonance imaging

CT: Computed Tomography

GIB-UB: Biomedical Imaging group

LB: Lewy Bodies

UPDRS: Unified Parkinson's Disease Rating Scale

ROIs: Regions of interest

MC: Monte Carlo

AI: Artificial intelligence

CNNs: convolutional neural networks

GANs: generative adversarial networks

EANM: European Association of Nuclear Medicine

FSL: FMRIB Software Library

SPM: Statistical Parametric Mapping

FBP: Filtered Back Projection

ANTs: Advanced Normalization Tools

HD-BET: High Definition Brain Extraction Tool

BET: Brain Extraction Tool

FAST: FMRIB's Automated Segmentation Tool

FIRST: FMRIB's Integrated Registration and Segmentation Tool

xAAL: Extended Automated Anatomical Labeling (atlas)

SSIM: Structural Similarity Index Measure

MSE: Mean Squared Error

FDA: Food and Drug Administration (USA)

MDR: Medical Device Regulation

GDPR: General Data Protection Regulation

DICOM: Digital Imaging and Communications in Medicine

NIfTI: Neuroimaging Informatics Technology Initiative

BIDS: Brain Imaging Data Structure

Table of contents

1. Introduction

Parkinson's disease (PD) is a chronic, progressive neurodegenerative disorder affecting the motor and nervous systems. Symptoms include involuntary tremors, muscular rigidity, slowed motion, and psychological issues such as depression, anxiety, and memory problems. As PD advances, it leads to significant disability and care needs. PD is the second most common neurodegenerative disorder after Alzheimer's disease, with increasing prevalence and mortality rates. [1]

PD is characterized by the loss of dopaminergic neurons in the substantia nigra pars compacta (SNpc), resulting in reduced dopamine in the striatum, causing motor symptoms. [2] Typically, PD diagnosis is based on clinical evaluation. However, emission tomography imaging, including Positron Emission Tomography (PET) and Single Photon Emission Computed Tomography (SPECT), serves as a valuable tool to enhance PD diagnosis, monitor disease progression, and evaluate treatment efficacy. Specifically, SPECT using the radiotracer [123I] FP-CIT (commercially known as DaTscan) is useful for evaluating dopaminergic neurons. [3] [4] Moreover, even if brain SPECT scans are typically interpreted by the professionals' visual inspection, the quantification of these images can significantly enhance diagnostic accuracy.[5] This quantification involves measuring the uptake of specific radioligands in the striatal region, expressed through metrics such as the Specific Uptake Ratio (SUR), which will be defined in the 'Background' section.

1.1. Motivation

Lately, an increase interest in 123I-Ioflupane[1] quantification methods to numerically evaluate radioactive distribution in the nigrostriatal region has been observed, leading this to the release of several quantification methods collected in commercial software. These tools are already being used in clinical settings, as they undergo a validation process required for CE marking, typically based on comparison with the patient's clinical profile. [6] However, their generalized and robust use is still limited due to the lack of reliable gold standard references that would allow for objective validation of their quantification accuracy.

The motivation of this project lies in the need to develop reliable and precise systems that enable the proper assessment of the quality and vericity of specific medical imaging quantification methods. These techniques require the obtention of reference images to serve as ground truth, which can be generated through simulation. Among the few available options (as will be discussed in the Market Analysis section), there is SimSET, a simulation engine designed to simulate images from user-defined maps [7]. The goal of this software is to enable the modeling of any SPECT scan specified by the user applying Monte Carlo methods, computational algorithms that use random sampling to estimate numerical results. [8]

[1] 123I-Ioflupane is an equivalent nomenclature for referring to [123I] FP-CIT (also known as DaTscan)

1.2. Objectives

The main objective of this project is to develop a simulation pipeline capable of generating **realistic** SPECT images with known ground truth using Monte Carlo methods.

In line with this goal, a series of secondary objectives have been established to address the specific requirements of the proposed pipeline:

- Prepare it to allow an iterative process in the simulation calculus.
- Adapt it to SimSET architecture.
- Test its performance with a dataset of real images.

Derived from the handling of a dataset, other aims are defined:

- Depuration and optimization of the preprocessing codes involved in the framework.
- Inclusion of quality control checkpoints to ensure dataset integrity and traceability throughout the pipeline.

1.3.Scope

According to the objectives described above, this project lays the groundwork for the development of a simulation-based pipeline that enables the generation of realistic SPECT studies. The ultimate aim is to build the foundation for a future database of realistic simulated studies with known ground truth, which will allow the evaluation and benchmarking of different quantification and/or image processing methods intended for clinical implementation, including acquisition and reconstruction algorithms. The project focuses on the simulation of the dopaminergic system using [123I] FP-CIT as the radiotracer for SPECT imaging. While the current work does not aim to produce a final applicable tool, it represents an essential first step toward establishing a reliable framework that can support future validation of medical imaging software under controlled, reproducible conditions.

1.4.Methodology

The project is based on the implementation of an **iterative** pipeline for generating realistic simulated SPECT images using Monte Carlo techniques. The process begins with the conversion and organization of clinical imaging data into a standardized format suitable for automated processing. Subsequently, relevant brain regions are segmented from magnetic resonance images (MRI) and registered with corresponding computed tomography (CT) scans to generate attenuation and activity maps. These maps serve as inputs for the simulation engine, which generates synthetic projection data emulating clinical acquisition conditions. The simulated projections are reconstructed and then compared with clinical reconstructions to evaluate their level of similarity. Based on this comparison, the activity map is adjusted to generate new simulations, repeating the process iteratively until a satisfactory level of similarity between simulated and clinical images is achieved.

1.5.Location of the project

This project has been conducted in collaboration with the Biomedical Imaging group (GIB-UB) of the Biophysics and Bioengineering Unit from University of Barcelona (UB). This is a highly experienced research group specialized in the development of software for treatment, and study of biomedical images, including nuclear medicine simulation, the main line of research of this project. The project has been primarily developed in the Biophysics and Bioengineering Laboratory of the Faculty of Medicine at UB, although remote work has also been conducted.

2. Background

2.1.Parkinson's disease

Characteristics and symptoms

PD is a chronic, progressive neurodegenerative disorder primarily affecting the motor system but also impairing cognitive processes, emotional regulation, and autonomic functions. Its main clinical signs are often summarized using the acronym TRAP: [9]

- Tremor at Rest: Involuntary shaking, especially in the hands and arms, observed in about 70% of PD patients as the first symptom. [10]
- Rigidity: Increased stiffness and resistance during passive joint or limbs movement. [10]
- Akinesia: Loss of movement, associated with bradykinesia (slowness of movement) and hypokinesia (reduced movement). [10]
- Postural Instability: Gradual loss of balance due to impaired postural reflexes, leading to an increased risk of falls, generally appearing in the later stages of PD. [10]

PD has a prevalence of 0.3% in the general population, with prevalence rising to 1% among people over 60. It rarely occurs before age 50, affects individuals of all ethnicities, and is slightly more common in men. [11]

Etiology and pathology

The exact cause and molecular mechanisms of PD remain still unknown. [12] While about 95% of cases are sporadic with no genetic linkage, the remaining cases are linked to genetic mutations, such as those affecting the parkin gene. [13] PD is thought to result from a combination of aging, genetic factors, and environmental exposures. [14] The hallmark features of PD pathology include the loss of dopaminergic neurons in the SNpc and the presence of Lewy Bodies (LB). [10] [13] [15]

Dopaminergic Neurotransmission System

As mentioned, PD primarily affects the dopaminergic neurons, which produce dopamine and are crucial components of the basal ganglia, including the striatum, nucleus accumbens, globus pallidus, subthalamic nucleus, and substantia nigra *(see Figure 1)*. The basal ganglia is involved in motor control as well as cognitive and emotional functions. [11] In PD, the degeneration of SNpc dopaminergic neurons disrupts the basal ganglia circuitry, leading to motor symptoms. [16] [17]

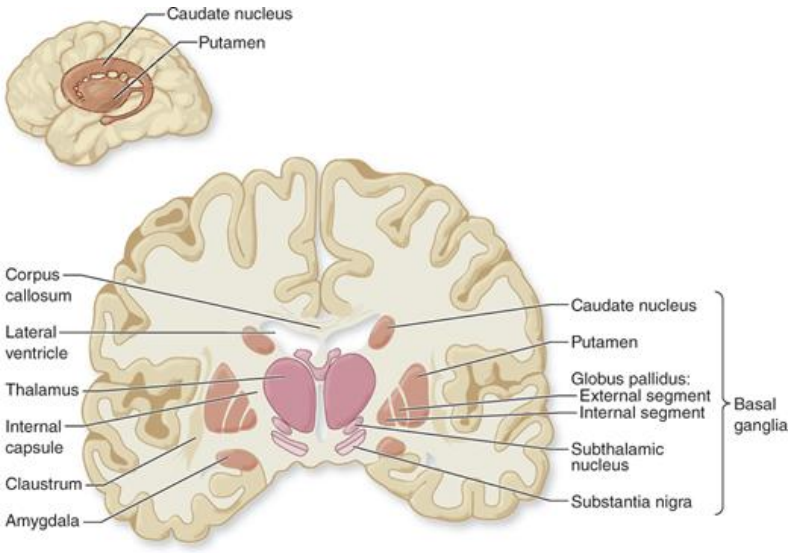

Figure 5. Overview of the components of the basal ganglia in coronal view. [18]

The nigrostriatal pathway, which transmits dopamine from the SNpc to the striatum, is crucial for motor control. The degeneration of this pathway results in the primary symptoms of PD. Dopamine synthesis occurs in dopaminergic neurons and is regulated by the Dopamine Transporter (DAT), which controls dopamine levels by reuptaking excess dopamine from the synaptic space. In PD, reduced dopamine leads to decreased DAT, serving as an indicator of dopaminergic neuron degeneration. [14] [11] [19]

Diagnosis and progression

The diagnosis of PD is primarily clinical, based on characteristic motor symptoms and secondary signs. Although there are no definitive biological markers for PD, sustained improvement with levodopa treatment supports the diagnosis. Post-mortem examination remains the gold standard for confirming PD, identifying the loss of nigrostriatal neurons and the presence of LB. [20] [21] To assess motor impairment and disability, scales such as the Hoehn and Yahr scale and the Unified Parkinson's Disease Rating Scale (UPDRS) are used. The Hoehn and Yahr scale, widely utilized worldwide, categorizes PD severity into five stages, providing a framework for comparing patient groups and tracking disease progression. [22] [23]

2.2.SPECT imaging technique

SPECT technique has contributed to a better understanding of PD as it allows the in vivo assessment of the dopaminergic neurotransmission system.

SPECT imaging is a diagnostic technique in nuclear medicine. It involves administering a small amount of radioactive substance attached to a specific compound, known as a radiotracer or radiopharmaceutical, which travels to the target organ or tissue. As the radiopharmaceutical decays, it emits gamma rays that are detected by a gamma camera positioned over the body part being studied. This process creates an image showing the distribution of the radiopharmaceutical within the body. [25] [26]

Radiotracers for Parkinson's Disease Diagnosis

Iodine-123 labelled 2-iodo-6-methoxybenxamide (IBZM) was the first SPECT tracer used to study dopamine postsynaptic receptors in (PD). Over time, other presynaptic dopaminergic terminal SPECT ligands like [123I] FP-CIT and [123I] β-CIT have been introduced into clinical practice. [123I] FP-CIT, also known as DaTSCAN, is the most used presynaptic radioligand. It binds to presynaptic dopamine DAT and detects changes in striatal uptake in patients with premotor PD symptoms and asymptomatic carriers of genetic mutations in familial PD. Its rapid uptake kinetics allow SPECT imaging 3 to 6 hours after administration, and its high affinity and specific binding to DAT make it ideal for clinical use. SPECT imaging with DaTscan provides a 3D image of the striatal dopaminergic system, useful for detecting the loss of nigrostriatal dopaminergic neurons. This technique is particularly valuable for distinguishing PD from essential tremors and differentiating LB dementia from Alzheimer's disease. In PD and LB dementia, there is **reduced uptake in the striatal region**, indicating a loss of dopamine transporters *(see Figure 2)*. [27]

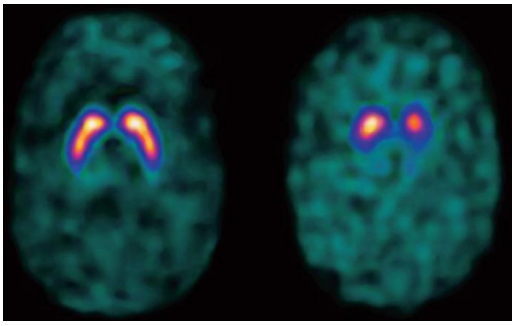

Figure 6. DaTscan of a normal patient (left) and DaTscan of a patient with Parkinsonian syndrome (right) [28]

Image Acquisition and Reconstruction

The gamma camera captures 2D projections from different orientations. Multiple detectors, typically ranging from one to four, rotate around the patient to acquire projections from various angles. As the gamma camera rotates, it collects projection profiles at each angle, generating a data matrix called a sinogram. Each row in the sinogram represents an intensity profile across an angular view, creating a sinusoidal pattern. [29] [30] *(see Figure 3)*

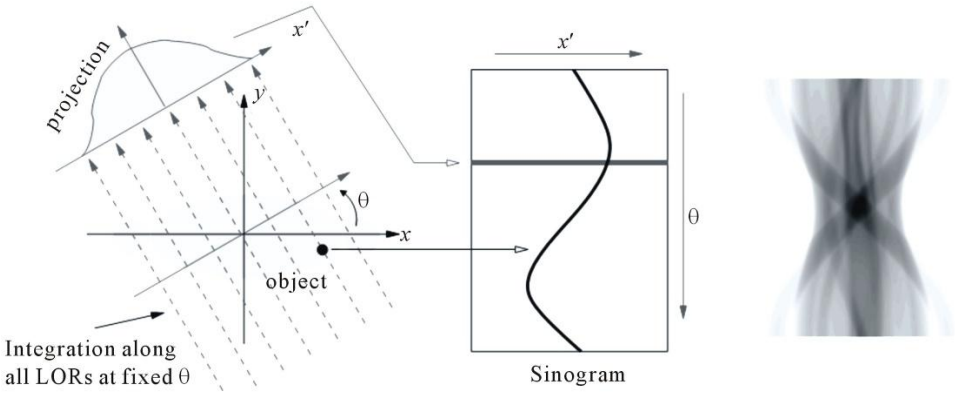

Figure 7. Tomographic acquisition process based on projections and sinogram formation [31]

To visualize the 3D results, the sinogram must be reconstructed. The reconstruction process involves transforming the sinogram into a volumetric image that represents the radiotracer distribution within the patient. This transformation relies on combining the projection data collected at different angles to estimate the internal activity distribution. The goal is to recover a spatially accurate representation of the radiopharmaceutical uptake, enabling both visual assessment and quantitative analysis. While various reconstruction algorithms exist, the process in general serves as a bridge between raw projection data and clinically interpretable images. [32] *(see Figure 4)*

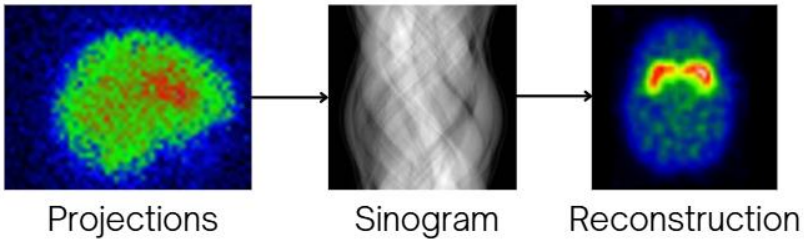

Figure 8. Process of the obtention of a SPECT study (Own source)

Quantification

There are different methods to quantify SPECT images, but the semi-quantitative method is highly recommended to objectively assess DAT binding. Quantification is performed using different Regions of Interest (ROIs), which can be defined either on high-resolution MRI images of the same patient or in a standard space using a template. Semi-Quantification uses the equation below to calculate the SUR in order to quantify radioligand uptake in the striatal volume *(see Equation 1).*

$$SUR = \frac{\overline{A_s} - \overline{A_0}}{\overline{A_0}} \qquad \textit{(Equation 1)}$$

A_s is the mean activity concentration in the striatal region and A_0 is the mean activity concentration in a reference region (typically the occipital area, which is free from radioligand uptake). [33]

2.3.State of the art

As previously explained, quantitative image analysis requires a reference or ground truth to evaluate how accurate the results are.

A traditional way to get this reference is by means of using **physical phantoms**, objects built to imitate human tissues and scanned with real equipment. The procedure consists of filling the phantoms with a specific activity, representing that of the brain, and introducing them into the gamma camera to acquire the images that will be later on quantified. Since the structure of the phantom is fully known, it serves as a comparison point. This process is represented in *Figure 5*. Although phantoms provide accurate validation, they have some limitations. The process is time-consuming and labor-intensive. Also, they are hard to modify, especially when trying to reproduce complex geometries like those in the human brain. Their rigid design makes it difficult to model specific conditions or patient variability, which often leads to reference images that do not fully reflect real clinical scenarios. [32]

Because of this, **simulation** has become a powerful and more efficient alternative. In a simulation, the phantom is created digitally, giving full control over its shape, composition, and internal activity. This allows researchers to design highly detailed models that represent different brain structures, disease stages, or technical setups. Simulations can generate a wide range of realistic scenarios without needing a physical scanner, reducing both costs and time, while offering greater flexibility and accuracy for method validation. [33] To implement numerical phantoms with an activity and attenuation map in simulation softwares the same procedure is applied but performing a simulation instead of an acquisition *(see Figure 6)*.

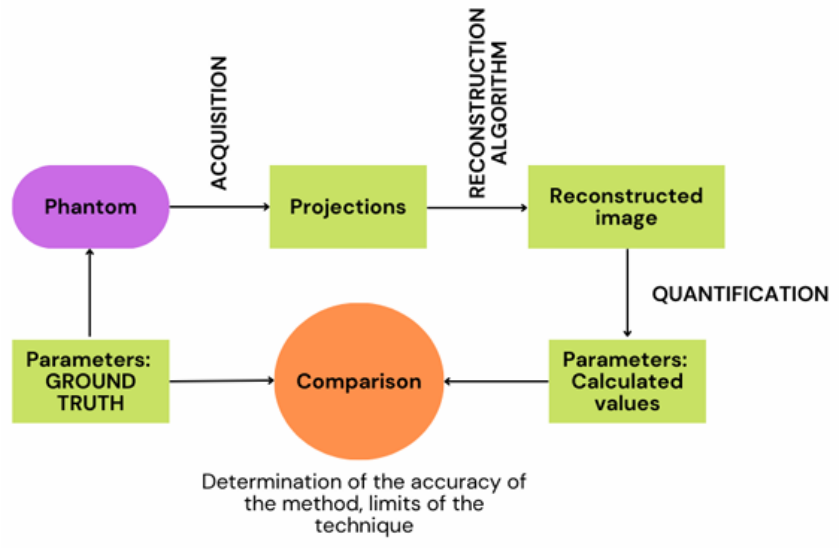

Figure 9. (Left) Process of evaluating quantification through phantom image acquisition. (Own source)

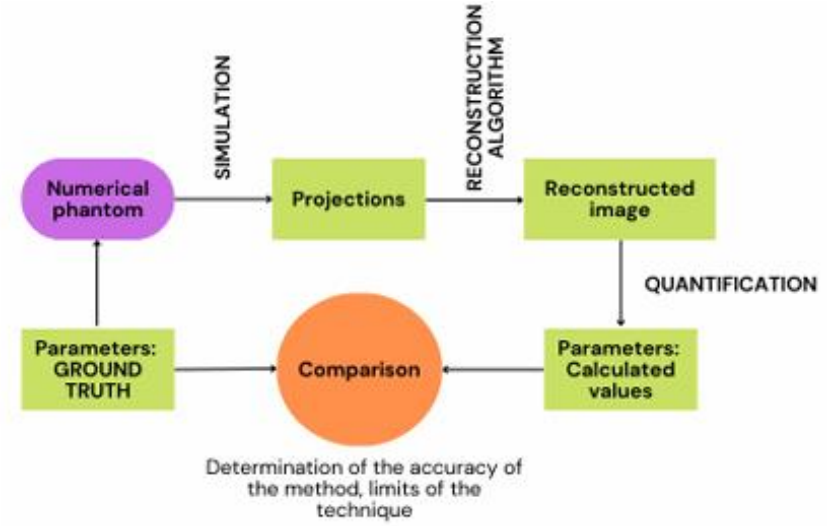

Figure 6. (Right) Process of evaluating quantification through simulation softwares. (Own source)

Monte Carlo (MC) simulation is a computational method that uses probabilistic models to estimate the likelihood of different outcomes for random variables. The method is named after the Monte Carlo Casino in Monaco, reflecting its association with randomness and games of chance. This technique is particularly useful for simulating physical processes in SPECT imaging, allowing for the generation of synthetic data without the need for physical phantoms, making it a cost-effective alternative for validation. The simulation mimics the emission and attenuation of gamma rays in biological tissue, as well as the collimation and detection processes of the imaging system. Given the stochastic nature of radiation emission, transport, and detection, the MC method is widely regarded as one of the most accurate for these applications. [8]

In addition to Monte Carlo, based methods, deterministic or analytical simulation approaches have been explored. These rely on mathematical approximations, such as projection and backprojection models or convolution operations, to replicate image formation. Although they are less realistic from a physical modeling standpoint, they offer much faster computation times and are often used in algorithm prototyping or training scenarios. [34] More recently, artificial intelligence (AI)–driven methods have emerged in the simulation landscape. Deep learning models, particularly convolutional neural networks (CNNs) and generative adversarial networks (GANs), are being used to generate synthetic SPECT images, correct for attenuation, or enhance image quality. These data-driven models can produce realistic outputs rapidly once trained and have shown promising results in reducing noise [35].

3. Market analysis

3.1. Target Sectors

The primary intention of this pipeline is to be used in order to generate a realistic database of simulated SPECT studies, particularly tailored to support the validation of quantitative image

analysis methods in neuroimaging applications such as Parkinson's disease. These synthetic datasets are highly valuable across multiple domains where reliable ground truth is essential for validating different image processing techniques, including acquisition, reconstruction and quantification techniques.

The project has been developed in the field of nuclear medicine imaging, with a special emphasis on quantitative SPECT applied to neurodegenerative disorders. However, its impact extends to two related markets. These include academic and clinical research institutions working on novel processing pipelines and companies developing medical imaging software.

Research groups are frequent users of simulated imaging data, particularly in early-stage method development. Projects like the EU-funded SIMCor initiative have shown the value of in silico trials for medical device evaluation through realistic virtual cohorts [36]. In nuclear medicine, platforms like SimPET have provided Monte Carlo-based PET datasets for validating quantification and registration methods [37]. Regarding SimSET specifically, several research groups are currently taking advantage of it in their studies; some examples are: the University of Washington, which, apart from developing the tool, is working with it [7]; the Department of Biomedical Engineering of the University of California-Devis [38] or the department where this project has been developed, the GIB-UB.

Both **software developers and commercial imaging vendors** working on diagnostic tools and quantitative analysis platforms also benefit from such resources. Companies like Voximetry [39], Subtle Medica [40] and Mirada Medical [41] increasingly rely on simulated data to train, test, fine-tune and validate their algorithms, reducing dependency on expensive clinical acquisitions and expediting regulatory approval. Similarly, vendors such as MIM Software [42] and Hermes Medical Solutions [43] incorporate simulated data into their development and quality assurance workflows to support the validation and deployment of clinical imaging tools. Moreover, for AI-driven imaging tools, large and diverse datasets, real or simulated, are essential for model generalization and reproducibility.

Although the final goal of the realistic database in question is to support the validation of clinical software, it is important to note that hospitals and clinics typically adopt commercial tools that have already been validated externally. Internal validation by healthcare providers is uncommon, which further emphasizes the need for high-quality public simulation resources for software vendors and regulatory assessments.

Beyond commercial stakeholders, professional organizations such as the **European Association of Nuclear Medicine (EANM)** [44] play a central role in shaping clinical practice, research priorities, and technological adoption in the field. While not a direct customer, the EANM represents a valuable communication and dissemination platform for innovations in image quantification and simulation. Engagement with such entities can foster validation, visibility, and eventual integration of advanced tools into clinical workflows.

3.2.Historical Market Evolution

The trend towards quantification in SPECT imaging has been evident since the first methodological approaches in the 1970s. Tools that provide accurate quantification, particularly for SPECT, are increasingly in demand for both clinical diagnostics and research. The development of dedicated software solutions, such as those integrated into GE **DaTQUANT**, reflects the growing interest in robust quantification tools for DaTscan imaging. Released by GE Healthcare in 2013, this software automatically calculates putamen-to-caudate uptake ratios using predefined VOIs and enables longitudinal monitoring of disease progression. [45]

As explained before, validation of these methods, including acquisition protocols and reconstruction techniques, is essential and can be done using phantoms or simulations.

These are some examples of the phantoms that are commercially available.

- **Hoffman 3-D brain phantom** *(Figure 7)* is crafted by CAPINTEC and it offers a precise three-dimensional replication of radiopharmaceutical distribution within the brain, tailored for SPECT and PET investigations. Its primary functions include assessing acquisition and reconstruction techniques as well as quantitative methodologies [46].

- The **Striatal Phantom**, depicted in *Figure 8*, is designed to enhance the quantitative accuracy of PET or SPECT imaging in clinical settings. This phantom is modeled on a standard RSD head with a cut in the calvarium to easily insert or remove the brain shell. Its purpose is to gauge image fidelity and validate quantification of striatal uptake. It comprises a brain shell divided into five compartments for separate filling: left and right nucleus caudate, left and right putamen, and the remaining brain tissue [47]

Figure 7. (Right) Hoffman 3-D Brain Phantom cylinder and 3-D Brain Insert [46]

Figure 8. (Left) Striatal Phantom [47]

On the other hand, over the last three decades, a variety of Monte Carlo–based simulation tools have emerged to support emission tomography, both for PET and SPECT modalities. Originally conceived to model radiation transport in nuclear environments, several of these simulators were later adapted to the medical imaging field as the demand for accurate, customizable simulation environments grew. These platforms have evolved from academic prototypes to widely adopted resources in research and, in some cases, clinical development.

- One of the earliest and most influential tools is **MCNP (Monte Carlo N-Particle)**, developed by Los Alamos National Laboratory, which became available to researchers in the 1980s. Although initially focused on general radiation physics, MCNP's flexibility allowed it to be adapted to emission tomography studies. [48]

- In parallel, the **SimSET** platform was released in the early 1990s by the University of Washington Imaging Research Laboratory, specifically tailored for PET and SPECT simulation using voxelized anatomical inputs. Its academic license and efficient computation made it a valuable resource for research applications. [7]

- In the 2000s, a new generation of simulation software emerged, combining greater physical realism with modular programming. **GATE**, developed by the OpenGATE collaboration in 2004, is perhaps the most prominent example. Built upon the Geant4 particle physics toolkit, GATE enabled highly flexible simulations of time-dependent imaging processes, including PET, SPECT, CT, and even radiotherapy scenarios. [49]

- Around the same period, **SIMIND**, developed by the medical physics group at Lund University Hospital in Sweden, was also gaining traction. It offers a SPECT-specific solution known for its user-friendly interface and strong alignment with clinical protocols. [50]

- More recently, newer simulation tools and platforms have expanded the market. **STRATOS**, developed for rapid prototyping and image simulation, has been adopted in experimental setups where faster iteration cycles are needed. [51]

- PET-focused simulators such as **SimPET**, MCGPU-PET (Monte Carlo GPU-based Positron Emission Tomography) and ASIM (Analytic PET Simulator) provide alternatives optimized for performance and accuracy in brain imaging or small-animal studies. Some platforms, such as SimPET, even offer web-based simulation services to enhance accessibility and reproducibility. [52] [53]

3.3. Future Market Perspectives

Despite significant advancements in SPECT simulation, the synthetic images generated to date are not fully realistic when compared to clinical acquisitions. Even when simulations are based on attenuation and activity maps extracted from real patient data, these maps are custom-designed and often fail to capture the true distribution patterns observed in actual SPECT studies, particularly in terms of regional uptake ratios such as SUR. This discrepancy limits the usefulness of such simulations for validating quantitative methods. Therefore, the future market perspective is the development of different pipelines, such as the proposed in this project, to improve the realism of the synthetic images obtained from the simulation tools mentioned above.

One of the most relevant precedents in this area is the Brain-VISET project (Voxel-based Iterative Simulation for Emission Tomography), a collaborative initiative led by the Instituto de Investigación

Sanitaria de Santiago de Compostela (IDIS) and the University of Santiago de Compostela (USC). Brain-VISET was specifically developed to support simulation and quantification in PET neuroimaging. The framework integrates anatomical and functional information extracted from real PET and MRI scans to generate synthetic PET datasets through Monte Carlo-based simulations, followed by image reconstruction with tools like STIR. Its voxel-level approach allows for precise control over activity and attenuation maps, resulting in synthetic images that closely replicate the statistical and physical characteristics of clinical acquisitions. [54]

The Brain-VISET methodology was originally developed for PET and integrated into SimPET. This project seeks to apply a similar process for SPECT imaging, where modular simulation frameworks are still uncommon. Brain-VISET has served as a key reference, demonstrating the potential of anatomically-informed iterative pipelines for generating realistic synthetic datasets.

Initiatives focused on SPECT are expected to emerge in the near future, following the same principles. However, deep learning approaches, such as image synthesis using generative models, are also gaining traction as alternative methods for producing realistic medical images without traditional physics-based simulation. While not yet mature enough to replace simulation entirely, AI-based techniques represent a promising direction for future image generation workflows.

4. Concept engineering

The aim of this final degree project is to create a pipeline capable of simulating and reconstructing realistic SPECT data by means of an iterative process. To accomplish this goal, the first step is to identify the appropriate tools necessary for developing the project successfully and consider the resources at disposal. Also, in this section several workable solutions are studied.

4.1. Dataset

In order to generate realistic simulated SPECT images, it is essential to work with real clinical data that can serve as a reference. For this project, a dataset of patients has been collected. It contains images from anonymized patients with Parkinson's disease diagnostic or suspicion, each including brain MRI, brain CT, and SPECT scans. The GIB-UB collaborates closely with Hospital Clínic de Barcelona, which facilitated access to this dataset.

4.2. Monte Carlo simulation

Given the advantages of Monte Carlo simulation in accurately modeling physical processes in nuclear medicine imaging, this project proposes a MC-based approach. Several Monte Carlo (MC) simulation platforms have been developed specifically for SPECT imaging, each offering different strengths. Among the most widely recognized are GATE, SIMIND, STRATOS, and MCNP, which have already been introduced in the Historical Market Evolution section. In order to choose the best

simulation engine for developing the pipeline, the availability and feasibility of each software is considered.

SimSET is a specific Monte Carlo simulator for emission tomography. It is a popular toolkit known for its computational efficiency and ongoing development. Although it does not support the advanced detector modeling features available in GATE, it offers excellent performance in scenarios requiring voxel-based input and high-throughput simulation. These features are particularly advantageous for pipelines that involve multiple simulation iterations. [7] Given that SimSET is already employed in the host laboratory (GIB-UB), it represents a highly practical and accessible option for this Final Degree Project. Its compatibility with existing data workflows, processing scripts, and cluster-based computing environments make it the strongest candidate for the development of an iterative pipeline.

In general, these simulation tools require two key inputs: an activity map that defines the spatial distribution of the radiotracer in the body, and an attenuation map that describes the tissue densities through which photons travel. In addition to these inputs, Monte Carlo simulators often rely on auxiliary configuration files that define simulation parameters such as detector geometry, collimator[2] specifications, binning strategy, and energy response. SimSET architecture is based on a photon history generator module, which simulates the trajectories and interactions of individual photons as they travel through the body and reach the detector. [7] The software architecture described is represented in *Figure 9*.

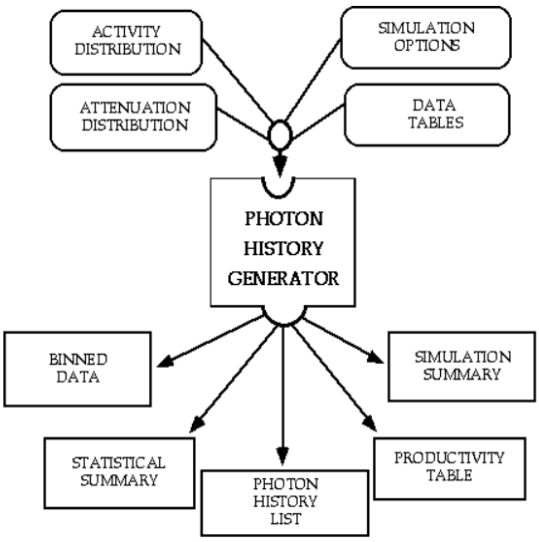

Figure 9. SimSET PHG inputs and outputs [7]

4.2.1. Attenuation and activity maps

Attenuation and activity maps are typically derived from anatomical imaging modalities such as MRI or CT, or generated synthetically when working with digital phantoms. Specifically, **T1-weighted MRI** scans are employed to create accurate anatomical segmentations, which are essential for defining the activity distribution within the brain. T1-weighted images provide high-resolution contrast between different brain tissues, making them ideal for accurate structural delineation. **CT** images, on the other hand, are used to derive attenuation maps due to their ability to provide quantitative information about tissue densities, which is critical for modeling photon attenuation accurately.

This project proposes generating these maps directly from the anatomical patient images included in the clinical dataset by processing them through a Python-based script. By integrating both T1-

[2] A collimator is a lead-based device in SPECT systems that allows only gamma photons traveling in specific directions to reach the detector, improving spatial resolution by blocking scattered or misaligned photons.

weighted MRI *(Figure 10, left)* and CT data *(Figure 10, right)*, high-fidelity simulations can be achieved.

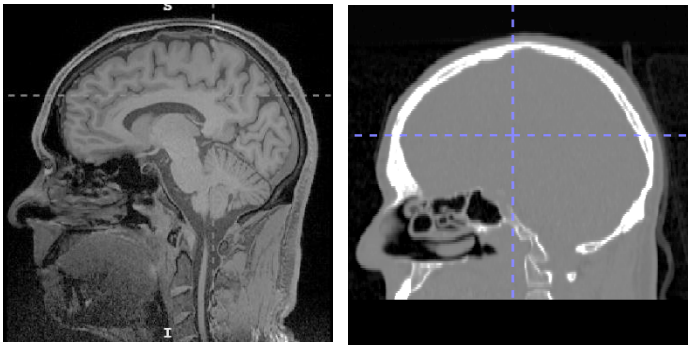

Figure 10. MRI (left) and CT (right) studies of one of the patients in the dataset (Own source)

MRI segmentation

To generate attenuation and activity maps from anatomical imaging, a critical first step is the segmentation of the brain MRI. This process allows for the extraction of relevant tissue classes and anatomical regions needed to construct input maps for simulation. Several established software tools are available for this purpose, each offering different advantages in terms of precision, processing time, and compatibility with automated workflows.

- Among the most widely used tools is **FSL (FMRIB Software Library)**, which includes modules such as BET for brain extraction and FAST for automated tissue classification from T1-weighted MRI scans. It is valued for its balance between accuracy and computational efficiency, as well as its ease of integration into Python-based processing pipelines [54].

- **SPM (Statistical Parametric Mapping)**, another popular tool, uses a probabilistic framework and a priori tissue probability maps to perform voxel-wise segmentation. It is well-suited for studies requiring spatial normalization and advanced statistical analysis, though its MATLAB dependency can complicate integration in some environments [55].

- **FreeSurfer** offers detailed cortical and subcortical segmentation, including surface reconstruction and morphometric measurements, making it a strong candidate for anatomical analysis; however, its high processing time may be a limitation in simulation workflows involving large datasets or iterative tasks. [56]

Therefore, the methodology to obtain attenuation and activity maps is the following: Starting from the MRI as the base image, masks generated from both MRI segmentation step and CT preprocessing are applied, in order to assign a specific attenuation or activity coefficient to each material or structure segmented. This results in the attenuation map and the activity map, respectively. Examples for this files are shown in *Figures 11 and 12*.

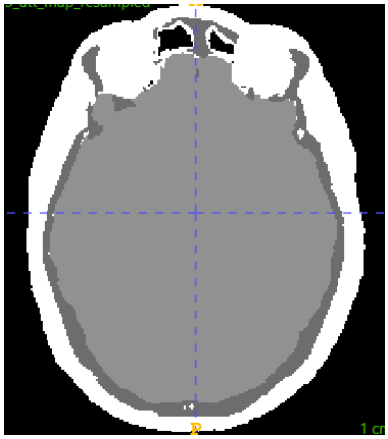

Figure 11. Attenuation map (axial view) (Own source)

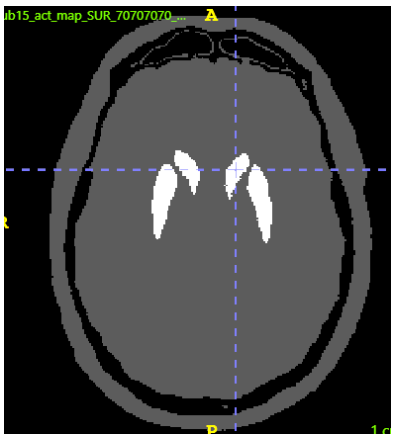

Figure 12. Activity map (axial view) (Own source)

The activity of interest in the clinical context of Parkinson's is that of the striatum. In simulations, it is typically defined by a 4-value SUR code (e.g., 70707070), with each pair of values indicating the relative activity of one of the structures present (left caudate, left putamen, right caudate, and left putamen). This SUR value is customizable by the user and can be specified both in the activity map before launching the simulation or later in the step prior to reconstruction.

Simulation setup

Simulation parameters are defined based on the specifications of the imaging system being emulated. Ideally, these parameters should match those of the gamma camera used to acquire the real SPECT images in the clinical dataset, in order to ensure that the simulated projections replicate the same acquisition conditions. This alignment strengthens the validity of the comparison between simulated and real data.

While hardware settings typically remain fixed, other simulation variables—such as acquisition time, tracer energy, and the number of photon histories—can be adjusted to better reflect different imaging conditions, such as the desired level of noise. SimSET allows the computation of free-noise simulations but these are computationally expensive and time-consuming, taking around 48 hours to finish. For this project, simulating with zero noise is not necessary, since the goal is to replicate real clinical studies, which are inherently noisy.

Moreover, it is possible to conduct two types of simulations in SimSET:

- **Independent simulation calculus for each structure:** This configuration allows the isolated inspection of each anatomical component being simulated (background, left and right caudate, left and right putamen and scalp). At the output, simulated projections are obtained separately and require a specific postprocessing to prepare data for reconstruction.

- **Simulation of the whole activity map:** This simplified approach simulates the entire activity map as a single structure. This method is not as computationally expensive as the previous one and is enough accurate for the purpose of this project.

4.2.2. Reconstruction algorithms

The simulation outputs include projection data in sinogram format and statistical summaries describing detection rates and photon histories. In order to perform a valid comparison between real and synthetically-generated data, it is crucial that both datasets undergo reconstruction using the same algorithm. This is because the reconstruction method itself introduces variability and any mismatch in reconstruction methodology could compromise the reliability of the comparison between clinical and simulated images.

Two main reconstruction methods for SPECT imaging data are widely used in clinical and research settings: analytical and iterative approaches.

● **Filtered Back Projection (FBP)** is an analytical method known for its speed, simplicity, and computational efficiency, making it widely used in clinical environments. FBP reconstructs the image by redistributing projection counts along the paths they were detected, applying a filter, commonly a Butterworth filter, to suppress high-frequency noise. Its advantages include minimal computational cost, rapid execution, and straightforward implementation, which are particularly beneficial in high-throughput clinical workflows or simulation pipelines requiring multiple reconstructions. Despite its strengths, FBP may be more prone to artifacts and reduced image quality in cases of low count statistics or non-uniform attenuation. [58]

● **Ordered-Subsets Expectation Maximization (OSEM)** is a widely used iterative reconstruction technique based on the Maximum Likelihood Expectation Maximization (MLEM) algorithm. OSEM refines the image estimate over multiple iterations by comparing measured and estimated projections, using subsets of data to accelerate convergence. Compared to analytical methods, iterative approaches like OSEM are more computationally intensive but offer enhanced noise suppression, better resolution recovery, and the ability to incorporate physical corrections such as attenuation and scatter modeling. [59]

In current clinical practice, both FBP and OSEM are routinely employed, with OSEM gaining traction for its superior accuracy in anatomically complex regions such as the brain. However, the simplicity, transparency, and computational efficiency of FBP continue to make it an attractive option, especially when reconstruction speed and reproducibility are crucial factors.

4.3.Iterative framework

To address the limited realism of the simulated images generated from the current softwares, this project proposes a strategy focused on iteratively improving the realism of activity maps. As explained before, these maps include different activity coefficients for the different anatomical structures that appear in the image. However, these distribution patterns are usually falsely uniform and homogeneous (see activity map in *Figure 12*) and do not accurately represent the ones observed in actual SPECT studies in terms of regional uptake ratios at the different regions of the brain. This discrepancy affects the realism level of simulated studies and limits the usefulness of such simulations for validating quantitative methods

The designed strategy involves comparing each simulated reconstruction with its clinical counterpart and adjusting the activity map accordingly. This iterative refinement is performed without tuning or modifying the internal parameters of the simulator itself, ensuring that improvements are solely driven by the adjustment of the input maps. As a result, the final simulations are expected to resemble more closely the physiological distribution of radiotracer uptake observed in clinical practice.

To perform the whole iterative process the following methodology is suggested. The procedure begins with the generation of an initial simulation based on attenuation and activity maps derived from the patient's MRI and CT images. Both the simulated and clinical projection data are reconstructed using the same reconstruction algorithm to ensure methodological consistency. Following reconstruction, both resulting images are aligned to allow for spatial comparison. To quantify the similarity between both reconstructed images, a numerical comparison metric is computed voxel-to-voxel as done in Brain-VISET [54].

In order to adjust the activity map, two solutions are considered:

One approach involves overlaying an anatomical brain atlas segmented into **predefined regions** onto the reconstructions. This atlas is first transformed from standard space to the patient space and resampled to match the reconstruction resolution. Once aligned, the atlas enables the calculation of average uptake values in each brain region for both the simulated and clinical images. The regional values from the two images are then compared by computing a ratio or difference for each atlas-defined region. These values are used to adjust the activity map: the brain atlas is overlaid onto the original activity map, and each region is scaled according to its corresponding ratio. This modified activity map is used as input for a new simulation, keeping all other parameters constant.

An alternative strategy considered for this step is a **voxel-wise** approach, where the ratio is calculated directly on a voxel-to-voxel basis across the entire brain volume. This method avoids potential loss of resolution and allows finer spatial sensitivity, which can be particularly useful when tracer uptake patterns are spatially heterogeneous. However, voxel-wise comparison can be more sensitive to noise and misalignment, and may require stronger spatial smoothing or regularization strategies. In contrast, region-based comparison offers increased robustness by aggregating voxel data, but might obscure localized differences, especially in regions with uniform uptake.

The process is repeated iteratively. At each iteration, the most recently generated activity map is modified and used to simulate the next projection set, which is reconstructed and compared again to the clinical reconstruction. This loop continues until the similarity between the simulated and real SPECT images reaches a predefined threshold, which serves as the stopping criterion for the iterative framework.

The whole process is schematically represented in *Figure 13*. It enables progressive refinement of the simulated data, with the ultimate goal of achieving reconstructions that are more closely aligned with clinical observations.

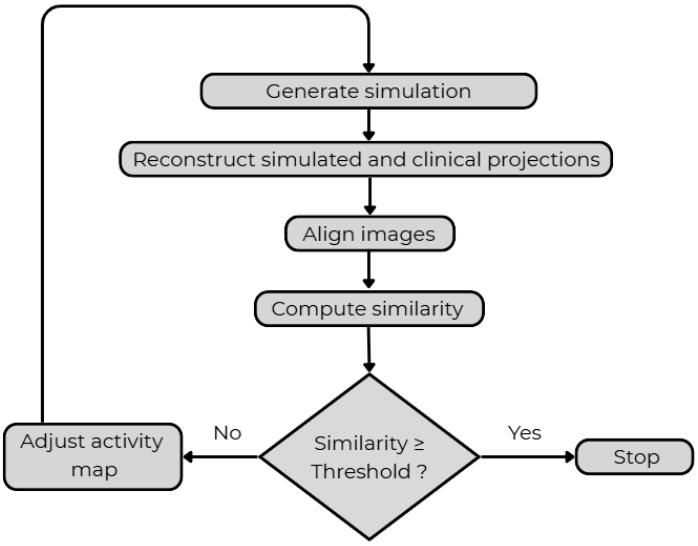

Figure 13. Schematic of the designed iterative process (Own source)

5. Detailed engineering

This project develops a pipeline to execute the iterative process described above *(see Figure 13)*. In this section, the different parts of this pipeline are described in detail.

5.1. Dataset preprocessing

As previously mentioned, the dataset created consists of 55 anonymous patients, each with available T1-weighted MRI, CT, and SPECT projection images acquired using one of the gamma cameras at Hospital Clínic de Barcelona. In some cases, the CT and SPECT acquisitions were performed simultaneously, meaning there is perfect spatial alignment between images of both modalities.

It is important to note that several patients were excluded from the dataset due to significant temporal gaps between the anatomical (MRI or CT) and functional (SPECT) studies. When an excessive time interval exists between acquisitions, anatomical changes may occur that compromise the accuracy of these modalities as anatomical references at the time of the SPECT scan. For the purposes of this simulation framework, it is critical that anatomical and functional data correspond to the same physiological state of the patient. Therefore, only cases with acceptable temporal proximity between imaging modalities were included. The studies included in the dataset were acquired between 2022 and 2024.

DICOM to BIDS (Brain Imaging Data Structure)

All images in the dataset were originally stored in DICOM format, which is the standard format used in medical imaging for storing and transferring image data along with embedded metadata. However, in order to facilitate further processing and analysis within modern neuroimaging workflows, it is necessary to convert DICOM files into the NIfTI format. NIfTI is widely adopted in research because it allows for more efficient access, manipulation, and compatibility with analysis software and libraries. To carry out this conversion, the executable tool dcm2nii.exe was used. While a more modern version of the tool, dcm2niix.exe, also exists and was tested, dcm2nii proved to be more compatible with the current Python-based pipeline developed for this project. [60]

Before starting their processing, all NIfTI images included in the dataset have undergone a visual quality control process to confirm the presence of the expected imaging modality and to ensure acceptable quality. Studies affected by artifacts or inadequate acquisition protocols were excluded in order to maintain the integrity of the dataset and avoid further problems in the next processing steps.

Each converted NIfTI file is accompanied by a corresponding .json file, which stores metadata extracted from the original DICOM headers using standardized DICOM tags. These tags include critical acquisition information that can be leveraged for simulation and quality control. In this project, the DICOM tags associated with the clinical SPECT studies are specifically stored and checked to ensure that the simulation parameters accurately reflect the clinical acquisition physical conditions. Examples of relevant DICOM tags include: acquisition time, acquisition date, scanner manufacturer, gamma camera model, patient orientation and position, image shape, pixel spacing, number of frames, etc. *(see Figure 14)*

AcquisitionTime	Manufacturer	StationName	StudyDate	AcquisitionDate
15:41:33	SIEMENS NM	GAMMA1	20230502	20230502
15:57:20	SIEMENS NM	GAMMA1	20230505	20230505
15:10:58	SIEMENS NM	GAMMA1	20230613	20230613
15:03:26	SIEMENS NM	GAMMA1	20230614	20230614
15:53:01	SIEMENS NM	GAMMA1	20230627	20230627
16:14:08	SIEMENS NM	GAMMA1	20230703	20230703
15:18:33	SIEMENS NM	GAMMA1	20230703	20230703

PatientOrientationCode	PatientPosition	RotationDirection	Rows	Columns	NumberOfFrames	PixelSpacing
Supine position	HFS	CW	128	128	384	3,895369768
Supine position	HFS	CW	128	128	384	3,895369768
Supine position	HFS	CW	128	128	384	3,895369768
Supine position	HFS	CW	128	128	384	3,895369768
Supine position	HFS	CW	128	128	384	3,895369768
Supine position	HFS	CW	128	128	384	3,895369768
Supine position	HFS	CW	128	128	384	3,895369768
Supine position	HFS	CW	128	128	384	3,895369768

Figure 14. DICOM tags (metadata) record from part of the dataset (Own source)

In this project, the dataset has been organized following the Brain Imaging Data Structure (BIDS) standard. BIDS provides a consistent, hierarchical structure for organizing neuroimaging data, enhancing reproducibility, interoperability, and clarity. Originally designed for MRI, BIDS has been extended to support CT and SPECT modalities, making it suitable for this multimodal dataset. [61] Each subject is stored in a sub-<label> folder, with modality-specific subfolders: rm/ for MRI, ct/ for CT scans, dat/ for SPECT images and dat_tc/ for multimodal SPECT and CT studies. An example of the BIDS architecture is represented in the image below *(see Figure 15).*

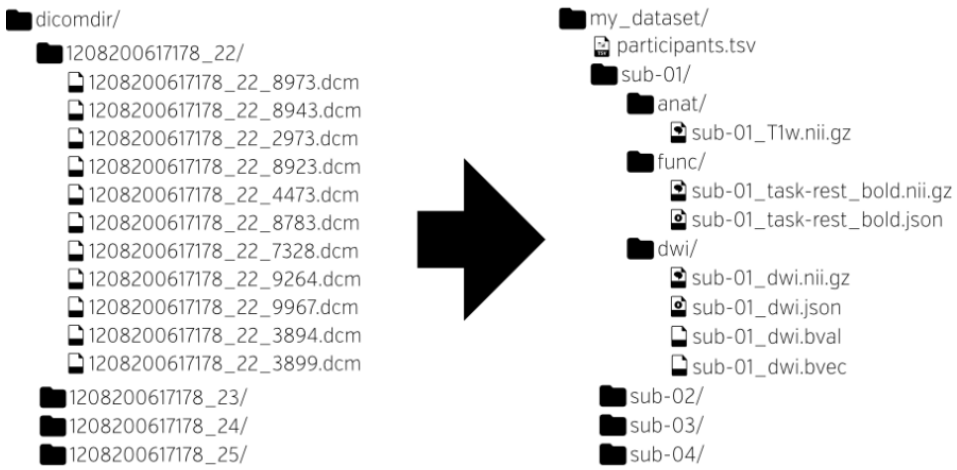

Figure 15. Example of BIDS architecture [61]

RM segmentation

The segmentation of brain MRI images in this project is mainly performed using the FSL suite. The initial strategy involved developing a Python-based program tailored to run on a Linux workstation in the Biophysics laboratory equipped with FSL.

For skull stripping, two methods are applied:

- **HD-BET:** It is a deep learning–based method providing high-accuracy brain segmentation, especially suitable for complex or noisy images, with optional GPU acceleration. [62] It provides highly accurate brain segmentation and returns, apart from the brain segmentation and mask in the original (patient) space *(see Figure 16)*, the segmented image transformed into standard space, which can be potentially useful in case spatial normalization is needed.

- **FSL BET:** It is a tool from the FSL suite that extracts the brain from MRI images by removing non-brain tissues like the skull and scalp [63]. It allows for manual adjustment of the brain extraction threshold and offers a robust option intended to improve segmentation in noisy or low-quality images. BET outputs, in addition to the brain segmentation and mask, a broader set of masks which are essential for constructing the attenuation and activity maps that serve as the foundation of our simulation pipeline. The masks generated are: an outskin mask (including the whole head of the patient), an outskull mask (just excluding the skin), a skull mask (including bone) and an inskull mask (including all the tissues inside the skull). *(see Figure 16)*

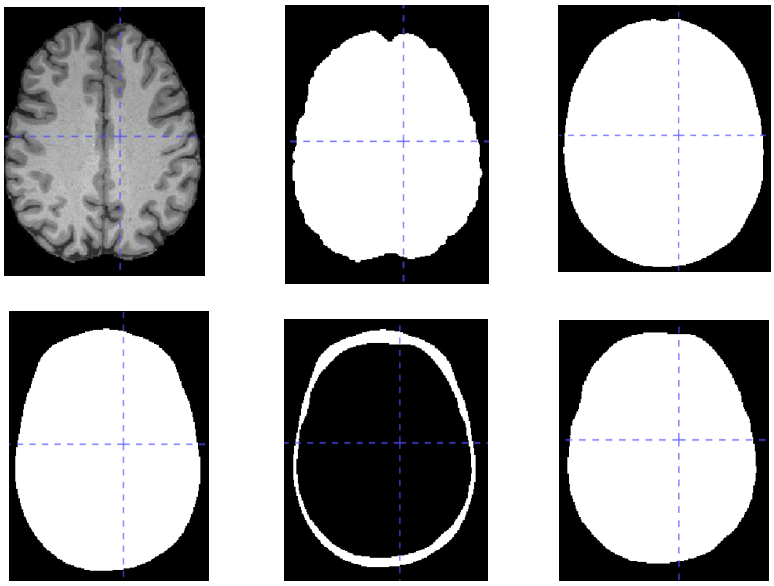

Figure 106. HD-BET brain segmentation (top left), HD-BET brain mask (top middle), outskin mask (top right), outskull mask (bottom left), skull mask (bottom middle) and inskull mask (bottom right). All images display an axial view of the head. (Own source)

A visual inspection of the results obtained from this segmentation step shows that BET does not correctly detect the brain in some subjects. Since BET output files are crucial for the pipeline's workflow several tests were conducted in order to improve the results. BET's robust mode was evaluated and different threshold values were tested but no significant improvement was observed. Finally, BET was tested in 3 different workstations with different versions of the software, resulting in more reliable segmentations using older versions.

Due to BET's limited accuracy, a quality control checkpoint was automated to systematically assess its performance across the whole dataset. This quality assessment checkpoint relied on the HD-BET segmentation as ground truth (which was considered as valid by previous visual inspection) and consists on comparing the number of voxels included in the BET-generated brain mask and the amount of voxels included in the one generated by HD-BET. Subjects exhibiting a large discrepancy in voxel count between the two methods were categorized as potentially poorly segmented by BET. These cases were subsequently reviewed through visual inspection, confirming that the masks generated by BET were inadequate. This quality control step helped identify and exclude suboptimal segmentations from further processing.

Additional segmentations are performed using FSL's FAST and FIRST tools.

FSL FAST (FMRIB's Automated Segmentation Tool) classifies brain tissue into three primary types: gray matter (GM), white matter (WM), and cerebrospinal fluid (CSF). Among its outputs, it provides an image where each tissue type is represented as a different intensity level (0 for CSF, 1 for GM, and 2 for WM) *(see Figure 17)*. Additionally, it generates binary masks for each class, probabilistic maps, and partial volume estimates, which express the likelihood or fractional content of each tissue type per voxel. These maps are key for localizing tissue boundaries and for quantitatively characterizing anatomical regions. [64]

FSL FIRST (FMRIB's Integrated Registration and Segmentation Tool) is used for subcortical structure segmentation, focusing on deep gray matter regions such as the caudate, putamen, globus pallidus, and thalamus. The tool employs shape and appearance models within a Bayesian framework, an approach that combines prior anatomical knowledge with image-derived evidence to estimate the most probable segmentation. [65] This allows FIRST to delineate these structures with high anatomical precision, even in the presence of image variability. Outputs include multiple individual NIfTI files for each structure as well as a combined NIfTI file containing all structures in a single labeled volume *(see Figure 18)*. Although FIRST typically expects a full-head T1-weighted MRI as input, in this project, the high accuracy of HD-BET was leveraged to preprocess the image. The brain segmentation obtained via HD-BET was used as the input to FIRST, taking advantage of the tool's option that allows specifying whether the input has already been brain-extracted. This modification improved segmentation outcomes by eliminating irrelevant regions outside the brain.

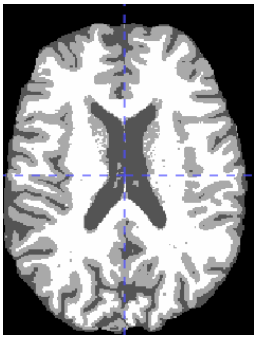

Figure 17. FAST output file representing brain tissues with different intensity levels (axial orientation) (Own source)

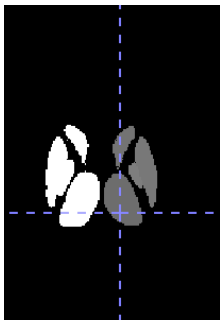

Figure 18. FIRST output file containing segmentation of subcortical structures (axial orientation) (Own source)

5.2.Attenuation and activity maps

As previously explained, to generate the necessary inputs for Monte Carlo SPECT simulation, two key maps must be constructed for each subject: the attenuation map and the activity map. These maps are created through a sequential Python pipeline that integrates multiple intermediate outputs derived from prior segmentation and image registration steps. The following section describes in detail the steps required to construct the input maps required by SimSET from our MRI and CT patient studies.

The workflow of the script is schematically represented in *Annex 1*. In the description below, some of the names of the files are included for ease of understanding.

1. **MRI-CT Co-registration:**

The first step is to align the CT image with the brain MRI using affine registration with ANTs (Advanced Normalization Tools), where the MRI serves as the fixed reference. ANTs is a widely used image registration toolkit known for its high accuracy and flexibility. [66] Affine registration is used here because it preserves linear spatial relationships while allowing for translation, rotation, scaling, and shearing, which are sufficient to align images like CT and MRI without distorting anatomical proportions [67]. MRI is used as the fixed image because it offers higher soft-tissue contrast and spatial resolution, especially for brain structures, making it a more reliable anatomical reference. In contrast, CT primarily captures bone structures and lacks the detailed contrast needed for precise alignment of brain tissue. This process outputs the aligned CT (ct_reg) and a transformation matrix.

2. **Removal of Support Structures:**

To isolate the head from the CT scan and remove the scanner bed or other artifacts, the registered CT image is multiplied by the outskin mask, resulting in an image without the surroundings (ct_reg_head).

3. **Attenuation Map Construction:**

The construction of the attenuation map integrates anatomical information from the binary masks obtained from segmentation and CT intensity values.

First, a labeled map is built where each voxel is assigned a value according to the corresponding anatomical region following these steps:

- Outskin mask is used as a base and, initially, the entire head is assigned 4
- The skull (obtained from the skull mask) is set to 5
- Inskull tissues (obtained from the inskull mask) are labeled as 6
- The brain (obtained from the HD-BET-derived mask) is labeled as 7

Then, a binary mask is generated from ct_reg_head and multiplied by the resulting labelled map to remove background values and exclude non-head regions. To refine the attenuation representation:

- Voxels with intensity >= 750 HU (Hounsfield Units[3]) in ct_reg_head are reassigned to value 3 (representing bone) in the output map.
- Voxels below -400 HU in ct_reg_head are set to 0 (representing air) in the output map.

The result is saved as _att_segmentation, containing detailed tissue-type labels.

[3] Hounsfield Units (HU) are a quantitative scale for describing radiodensity in medical CT images.

A simplified 8 bits version is created for SimSET compatibility, where muscle-equivalent tissues (current labels 4 and 5 representing outer skin and inskull non-brain tissues) are unified as value 7, bone is maintained with label 3 and brain is set to 4. This map is saved as _att_map and later used as simulation input. SimSET assigns predefined linear attenuation coefficients to each label in the input attenuation map, which correspond to materials such as air, bone, soft tissue, and muscle. By matching the values in our map to the expected SimSET labels (displayed in *Figure 19)*, we ensure that the physical properties modeled during photon transport simulation are realistic and correctly interpreted by the software.

```
Enter name of param file:
For this file, '/home/biofisica/simset-2.6.2.5/phg.data/phg_att_table'
        Using the attenuation index translation file
                /home/biofisica/simset-2.6.2.5/phg.data/phg_att_index_trans
        Your material indexes and names are:
                Index = 0, name = air
                Index = 1, name = water
                Index = 2, name = blood
                Index = 3, name = bone
                Index = 4, name = brain
                Index = 5, name = heart
                Index = 6, name = lung
                Index = 7, name = muscle
```

Figure 19. SimSET attenuation indexes for different materials (Own source)

4. Striatum Segmentation and Activity Labelling:

This is a previous step for generating the final activity map.

To generate binary masks of caudates and putamens, these components are identified from the segmentation of subcortical structures obtained from FIRST (all_fast_firstseg) and a binary mask is created for each structure.

These masks (created using _att_segmentation as basis, initial attenuation map) are then used to assign region-specific labels in the activity segmentation file (_act_segmentation), directly generated from copying _att_segmentation. This labelled map is used in the next step to assign an activity value to each structure.

Once the different regions masks are used to generate the labelled map, they are not needed anymore. Therefore, their further processing becomes optional and is only required in case the simulation is conducted processing each structure independently, which is not the instance of this pipeline. For this reason, even though the script generates outputs for this files, they will be no longer mentioned.

5. Activity Map Generation:

The correct execution of the iterative pipeline requires the activity of all anatomical components present in the image being established in the input activity map (before the simulation calculus), including the one of the striatum. As explained in previous sections, an 8-digit SUR code (e.g., '70707070') is used to encode the relative activity levels of four specific striatal regions: left caudate, right caudate, left putamen, and right putamen. Each pair of digits in the SUR string corresponds

to one of these regions and defines a relative activity intensity. Therefore, a SUR code with the same 2-digit number repeated four times indicates that all the striatum structures have the same uniform activity. All non-striatal tissues, such as muscle, scalp, or other brain regions, are assigned a uniform background activity value (10), while bone and air are assigned a value of 0 to reflect the absence of tracer uptake.

The activity value for each region is computed using the formula:

$$Activity_i = SUR_i + Activity_{background} \quad \textit{(Equation 2)}$$

where i indicates each striatal structure. This value is then assigned to all voxels in the corresponding region within a copy of the segmented activity map (_act_segmentation). According to SimSET requirements, original SUR digits must be ranging from 00 to 99 to represent a realistic, continuous and acceptable activity range.

This approach results in a custom-designed map that reflects physiological activity differences between structures, with striatum activity characterized by the chosen SUR code. The resulting map is saved as _act_map_SUR_{SUR_code} and an Excel file is generated to log the assigned activity values for each region, ensuring reproducibility and traceability.

To proceed with the execution of the Python script described, it is necessary to import specific modules from the FSL Python API. In particular, the script requires the module fsl.utils.image.roi, as well as the Image class from fsl.data.image. These components are essential for manipulating neuroimaging data and working with regions of interest (ROIs) within image volumes. Therefore, it is important to ensure that FSL is properly installed and configured in the Python environment before running the script.

6. Resampling to Simulation Resolution:

To conduct all simulations with the same geometry and uniform dimensions, activity and attenuation maps must be resampled to a fixed voxel size and volume dimensions. This involves three main steps:

1. Affine Definition and Resampling: Each image is resampled using Nilearn's resample_img function, with a new affine matrix that defines the desired voxel size of 0.859 × 0.859 × 0.9 mm and a final volume shape of 256 × 256 × 240 voxels. Nearest-neighbor interpolation is used, as the inputs are binary masks or labeled maps (e.g., _act_map_SUR_{SUR_code} and _att_map). This interpolation method preserves discrete values and avoids introducing partial volume effects. The Python function responsible for this step adjusts the affine matrix accordingly and casts the resulting data to 8-bit unsigned integers (uint8).

2. Cropping and Padding: Once resampled, images are either cropped or zero-padded to strictly match the target dimensions. If the resampled shape is smaller than the target (e.g., new_shape[0] = 252 vs. target = 256), padding is applied symmetrically: for a 4-voxel difference, 2 voxels are added before and after (i.e., pad = (-2, 254)), effectively instructing the cropping tool to extend the volume beyond its actual bounds by filling with zeros. Conversely, if the resampled image is larger than the target, excess voxels are cropped.

3. Consistent ROI Definition: For consistency in subsequent simulations and reconstructions, all maps are cropped with the same spatial indices derived from anatomical landmarks. This is especially important along the z-axis to avoid losing relevant brain regions or including non-cranial areas like the neck. Along the z-axis (inferior-superior direction), no padding is added below the neck, as simulating air under the patient would not be correct. This way we ensure anatomical structures remain centered and standardized across subjects.

This step is performed by two python functions; one to compute and record the pad and the other one to read this pad and apply the resampling. The padded or cropped dimensions are also logged for reproducibility.

Output files obtained from this step include both final attenuation and activity maps and both initial attenuation and activity maps labeled, all resampled to the target space for simulating.

7. Conversion to SimSET Format:

Due to SimSET requirements, all resampled maps are converted to .dat, .img and hdr Analyze-format[4] files and cast to uint8.

8. Resampling to reconstruction resolution

In addition to the simulation geometry, attenuation and activity maps are also resampled to match the resolution and geometry of the reconstructed SPECT images. This ensures that all reference data is also available in the reconstruction space for any potential alignment, evaluation, or comparison task that may be needed later in the analysis. This step may allow, for example, a future adjustment of the activity map directly in the reconstruction space.

The resampling is performed using the same Python-based utilities as in the simulation preparation stage, ensuring consistency in affine transformation and interpolation. Specifically, activity and attenuation maps that have already been resampled to simulation space undergo a second resampling. This is done by applying nearest-neighbor interpolation to preserve the discrete nature of the data. These maps are resampled to a fixed voxel size of 3.9 mm × 3.9 mm × 3.9 mm and volume shape of 128 × 128 × 56, matching the resolution of reconstruction space. The output files follow the naming convention: *_map_res_reco.

9. Template transformation

In some cases, it is useful to perform the full processing pipeline starting from templates in standard space. This allows for the possibility of reverting to standard space later in the workflow, should additional transformations or comparisons be required. For this reason, the processing of two standard-space templates is incorporated into the script: a whole-brain T1-weighted anatomical template *(Figure 20)* and an occipital region template *(Figure 21)*. The occipital region is specifically selected as it is commonly used as a reference in functional neuroimaging due to its anatomical

[4] Analyze-format files are an early neuroimaging data format consisting of a .hdr (header) and .img (image data) file pair.

clarity, relative stability in resting-state conditions, and preservation across various neurological disorders. This makes it a reliable region for normalization and comparative analysis. [33]

Both templates are first transformed into patient space. The T1 template is aligned using an affine transformation. The occipital template, in turn, is transformed using a generic label interpolator, as it contains discrete labeled regions; this method avoids interpolation artifacts and preserves the integrity of label boundaries. Once in patient space, both templates are resampled to match the simulation geometry. The occipital template is resampled using the same nearest-neighbor interpolation and voxel specifications used for attenuation and activity maps, ensuring consistency in spatial resolution and label preservation. The T1 template, being a continuous anatomical image, is resampled using continuous interpolation to preserve intensity gradients and anatomical detail. Finally, both resampled templates are further resampled into reconstruction space using the same methodology as in the previous resampling.

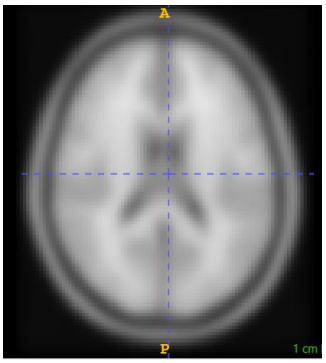

Figure 20. T1 template in standard space (axial view) (Own source)

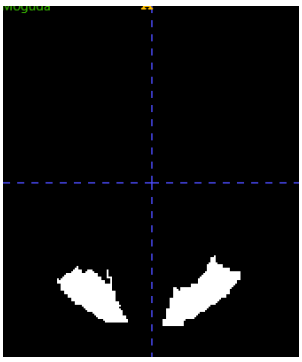

Figure 21. Occipital template in standard space (axial view) (Own source)

Lastly, to be ready for simulation, attenuation and activity maps of each subject must be adapted to the architecture of folders and filenames the simulator is expecting as input.

5.3.SimSET Simulation

As mentioned above, the chosen software engine to carry out the project is SimSET. This simulator is installed in a clustered workstation of the Biophysics and Bioengineering Laboratory. All simulations are launched from that workstation, a Linux-based high-performance computing (HPC) environment that operates through a node-based architecture. In this distributed computing model, tasks are executed across individual nodes, which act as semi-independent processing units within a shared infrastructure. To avoid interfering with other computationally intensive processes being run by other users on different nodes, all simulations are carried out in one of the available nodes, ensuring that they remain isolated and do not impact on the performance of parallel workloads within the system.

As previously mentioned, to closely replicate clinical SPECT studies, it would be ideal that simulation parameters describing the acquisition system are configured to match the physical characteristics of the gamma camera being emulated. In this project, the emulated acquisition

system is the gamma camera 1 specified in the DICOM metadata of the clinical scans performed at Hospital Clínic, which corresponds to a Siemens system.

On the other hand, indications for the simulation step of the pipeline include performing short (due to the time limitation of this Final Degree Project) and noisy simulations (to mimic real conditions). Noise level and simulation time can be both controlled by adjusting parameters such as the number of decays to simulate and the decay time. The number of decays to simulate determines how many radioactive disintegrations are generated, directly influencing the amount of statistical noise in the resulting projections. The decay time defines the total acquisition duration, which, in combination with activity levels, affects the event density. By lowering the number of simulated decays or shortening the decay time, we produce more realistic, noise-containing images that better reflect clinical conditions while also reducing computational cost and time. These modifications resulted in statistically balanced simulation outputs, as confirmed by the values reported by the simulation engine: the sum of accepted weights, which reflects the total contribution of all detected events, and the sum of squared weights, an indicator of statistical variance. These two values being of the same order of magnitude suggest that the simulation is not dominated by outlier events with disproportionate weights. Checking this balance is essential to ensure the simulated data are suitable for subsequent processing.

Nevertheless, since the methodology of this project is based on improving image realism through iterative simulations, it is not strictly necessary for the simulation parameters or the noise level to be fully optimized. The aim is not to achieve maximum realism from a single simulation run, but rather to progressively enhance realism by adjusting the activity map while keeping the simulation parameters fixed. As long as the simulation parameters remain the same, any increase in realism across iterations will depend solely on the modifications applied to the activity map. Starting from a reasonably realistic baseline is desirable, but what truly matters is the detection of a progressive improvement achieved in each iteration without the need of changing parameters related to the acquisition system characterization.

Regarding the simulation method, simulating each structure separately is not necessary for the purposes of this project. Therefore, the simplified approach in which the entire activity map is simulated as a single structure is adopted.

5.4. FBP Reconstruction

As previously discussed, it is important that both clinical and simulated projections are reconstructed using the same method, in this case FBP. This is particularly important because reconstruction is performed at every iteration of the workflow. If the activity map is progressively adjusted to enhance realism of simulated data, but the reconstruction method differs from the one used for the clinical data, additional variability is introduced into the process. Such inconsistency could undermine the improvements in similarity that the iterative activity map refinement is intended to achieve. Ensuring reconstruction consistency is therefore essential for maintaining the integrity and comparability of the results.

The basis of FBP reconstruction algorithm has already been explained in the Concept Engineering section. As mentioned there, a Butterworth Filter is applied before reconstruction to reduce high frequency noise that would otherwise be amplified by the ramp filter. The chosen parameters for the filter are a cut-off frequency of 0.5 and an order of 10. Also, FBP command itself applies a ramp filter to compensate for the blurring introduced by the back-projection step. It enhances high-frequency components and restores sharpness, ensuring the reconstructed image accurately reflects the spatial distribution of the activity. The specified parameters are used for both simulated and clinical reconstructions.

Simulated projections

A custom Python script has been developed to automate the complete post-processing and reconstruction workflow of the simulated projections.

This script integrates multiple processing stages into a single, consistent workflow. It begins by locating the relevant projection folders corresponding to each patient and SUR condition simulated. The simulation provides four types of projection files: primary photons, high-energy scatter, low-energy scatter, and the total projections file, labeled simply as 'projeccions'. Each file represents a different component of the detected signal: primary photons reach the detector without interaction, while the scatter components account for photons that have been deflected at different energy levels. Although the 'projeccions' file is theoretically the sum of all components, the pipeline explicitly reconstructs the image by adding the three individual components manually. This ensures maximum reliability and guarantees that the final input to the reconstruction accurately reflects the full projection data, as is the case in clinical studies. Once the components are summed, the resulting projection volume is normalized to a fixed target count value, estimated based on typical signal levels observed in clinical SPECT acquisitions. This normalization serves a dual purpose: it enforces consistency across simulations and reproduces realistic clinical count statistics, improving the comparability between simulated and real data. The normalized image is then rotated to match the correct acquisition orientation and cropped to extract the relevant region. After this geometric preparation, the Butterworth low-pass filter is applied. Filtered projections are then submitted to a custom FBP reconstruction module, which emulates the clinical reconstruction setup. Finally, the reconstructed volumetric image is saved alongside its header file. Throughout the process, header files are verified or regenerated to ensure compatibility with Analyze-format conventions.

This integrated script allows direct reconstruction of full-volume simulated activity maps that already encode the desired SUR configuration. The described process is summarized in Figure 22.

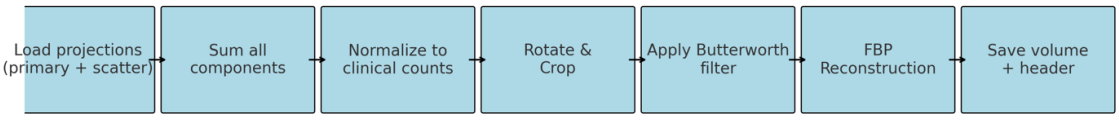

Figure 22. Reconstruction workflow for simulated projections (Own source)

Clinical projections

The reconstruction of clinical projections is carried out using a custom Python script that automates preprocessing and FBP reconstruction.

Although the same reconstruction method and exactly the same parameters are used for both clinical and simulated projections, ideally the same script would have been applied to both cases. However, this is not feasible due to the inherent variability of clinical acquisitions. The reconstruction script developed for simulated data assumes very specific structural features and a fixed format that are consistent across all simulated subjects. In contrast, clinical projections often require tailored preprocessing steps depending on the acquisition characteristics. As a result, the reconstruction of simulated projections is performed executing in an Ubuntu-based workstation the custom Python script described earlier, which internally calls a series of bash commands. In turn, the reconstruction of clinical projections is carried out on a Windows system using precompiled .exe executables. This dual-system setup, although not ideal, allows each type of data to be handled with the tools and platform best suited to its format and variability.

5.5. Iterative framework

The iterative process developed in this project (already introduced in the Concept Engineering section) relies on a **region-based approach** for adjusting the former activity map. A brain atlas divided into anatomical regions is used to quantify the difference between clinical and simulated images on a per-region basis. The resulting ratio from this comparison is then used to modify the activity map, which is resimulated in the next iteration. This feedback mechanism aims to progressively reduce the discrepancy between clinical and simulated data, enhancing realism in a structured and localized manner.

The first step in the framework is to generate the initial simulation, which is obtained from an activity map defined by the SUR code 70707070. In practice, the specific SUR value used at this stage is not critical, since the activity distribution will be iteratively adjusted as needed throughout the process. This is the selected value because it lies within the imposed range (00 to 99, considering a background activity of 10), providing a moderate initial contrast that makes the striatum clearly distinguishable and visibly enhanced in the first iteration. It is important to note that this uniform SUR configuration does not reflect real physiological distribution but serves as a functional starting point for the iterative refinement.

Reconstructions alignment

To accurately compare the clinical and simulated reconstructions, both images must be in the same spatial orientation and resolution. Since this project produces many simulated reconstructions in the native (MRI) space, one for each iteration, it is most practical to transform the clinical reconstruction to this common reference space. This way, the alignment step only needs to be performed once per subject, minimizing redundancy and ensuring consistency across iterations.

A dedicated Python script handles this realignment. The first step is to make the orientation of these reconstructions match. Then, the script uses the ANTsPy library [66] to register the flipped clinical image (moving) to the simulated reconstruction (fixed). Several transformation models have been tested for this task, including rigid, affine, and SyN (non-linear) registrations. The similarity transform is ultimately selected as it visually provides the best balance between accuracy and stability. This choice is particularly important, as the precision of this alignment step is critical: even small misalignments can compromise the validity of the region-based comparisons used to guide the activity map updates.

Anatomical atlas registration and resampling

The atlas used in this project for regional brain analysis is the **xAAL** (extended Automated Anatomical Labeling) atlas. This atlas is an enhanced version of the widely known AAL atlas, originally developed by Tzourio-Mazoyer et al. at the French neuroimaging research institute GIN (Groupe d'Imagerie Neurofonctionnelle). The xAAL version refines and expands the original labeling to offer better anatomical accuracy and broader coverage, particularly in cortical and subcortical areas. It segments the brain into well-defined regions using the standard MNI152 space, enabling consistent comparisons across subjects and studies. Its detailed parcellation makes it especially suitable for region-based quantification and image adjustment, as required by the iterative framework of this project.

Before using the atlas to guide either the similarity comparison or the modification of the activity map, it must be spatially aligned with the patient-specific data and resampled to match the resolution and dimensions of the simulation and reconstruction volumes. The atlas is initially in standard (MNI) space and thus must undergo registration and resampling to be usable within the iterative framework.

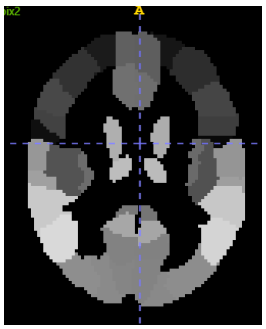

Figure 23. xAAL anatomical atlas (Own source)

A Python script accomplishes this task through a multi-step process:

1. **Registration to Patient Space**: The first step is to register the xAAL atlas, which is defined in standard space, to the patient's native anatomical space. This is achieved using the ANTsPy library. Initially, the registration was performed using the patient's T1-weighted MRI as the fixed image. However, since the T1 image includes extracranial and extracerebral structures that are not present in the atlas, which contains only cerebral regions, this led to suboptimal alignment. To address this, the T1 image has been replaced by a segmentation mask that includes only the brain, improving registration performance by ensuring spatial correspondence between both inputs. Several transformation models

have been tested, including rigid and affine registrations. However, the SyN (Symmetric Normalization) method is ultimately selected due to its superior performance in capturing both global and local anatomical variations, especially in deep brain structures. The xAAL atlas is treated as the moving image, and the subject-specific brain mask as the fixed reference. After computing the non-linear transformation, the atlas is warped into patient space using nearest-neighbor interpolation to preserve its discrete labeling. The result is a subject-specific atlas, spatially aligned to the patient's anatomy.

2. **Resampling to Simulation Space**: Once aligned to the patient space, the atlas is then resampled to match the resolution and voxel dimensions of the simulated projection data. This resampling involves adjusting the voxel size to a predefined resolution (0.859 × 0.859 × 0.9 mm) and applying a spatial padding specific to the patient, retrieved from a subject-specific Excel file generated from the maps generation code. The padding ensures that the final image fits precisely into the simulation volume dimensions (256 × 256 × 240).

3. **Resampling to Reconstruction Space**: Additionally, the script generates a second resampled version of the atlas to match the resolution and size of the reconstructed images. In this case, the resampling adjusts the image to a coarser resolution (3.9 mm isotropic voxels) and resizes the volume to 128 × 128 × 56 voxels, which corresponds to the FBP reconstruction setup. The appropriate padding for this transformation is again extracted from a separate subject-specific Excel file previously created.

In both resampling steps, the atlas data is first converted to uint8 to ensure compatibility, and nearest-neighbor interpolation is used to maintain the integrity of the label values. The final outputs are two patient-specific atlas images, one resampled to simulation space and the other to reconstruction space, that can be directly used for voxel-based operations in the iterative similarity framework. This preprocessing step ensures that the anatomical regions defined in the atlas are spatially valid and accurately overlaid on both simulated and clinical reconstructions.

Comparison metrics

Two quantitative metrics are established to evaluate the similarity between simulated and clinical images: the Structural Similarity Index Measure (SSIM) and the Mean Squared Error (MSE).

SSIM is a perceptual metric that quantifies image similarity by evaluating structural information, contrast, and luminance between two images. It is particularly useful in medical imaging, as it captures how similar the spatial organization of anatomical structures is between the simulated and clinical reconstructions. SSIM values range from -1 to 1, where 1 indicates perfect similarity. Since the SSIM metric does not directly support volumetric (3D) image comparison, the evaluation was adapted to a slice-by-slice approach. Specifically, the SSIM was computed independently for each axial slice of the images. For each slice, the values in the simulated and clinical reconstructions are extracted, SSIM is then calculated for these 2D slices and the resulting values are averaged across all slices to obtain a final, representative SSIM score. [68]

MSE, on the other hand, calculates the average of the squared differences between corresponding voxel intensities in the two images. It provides a straightforward estimate of pixel-wise dissimilarity,

where lower values indicate greater similarity. While MSE is sensitive to intensity differences, it does not account for structural or perceptual factors as SSIM does. [69] Since dealing with float images, MSE falls in the range between 0 and 1.

Together, these two metrics offer a complementary assessment: SSIM captures structural fidelity, and MSE reflects numerical accuracy.

In this project, similarity metrics are not computed over the entire reconstructed image but are restricted to the brain region. This decision is based on the fact that the iterative adjustments are applied exclusively to the brain activity map using a region-based brain atlas. As such, only the brain is subjected to modifications across iterations, and therefore it is the only region where improvement in similarity can be expected. Including the rest of the image, such as extracranial tissues or background, would introduce variability unrelated to the iterative process and could mask the actual impact of the activity map adjustments. In particular, structures that remain unchanged throughout the simulation (e.g., skull, scalp, or surrounding air) do not contribute meaningfully to the iterative refinement and may even bias the evaluation. For example, clinical SPECT acquisitions typically exhibit significantly more noise outside the patient due to acquisition conditions. This peripheral noise is not reproduced in the simulated images unless specific simulation parameters are specifically tuned to mimic it. Therefore, incorporating these regions in the similarity computation could lead to an underestimation of the improvement achieved in the brain. To ensure that the similarity metrics truly reflect the effectiveness of the activity map adjustments, the comparison is masked by a brain region defined by the same atlas used to modify the activity map. Achieving a more realistic match across the entire image, including extracranial noise, would require fine-tuning the simulator's configuration, which falls outside the scope of the current iterative framework.

Activity map adjustment

To implement the iterative adjustment of the activity map, a Python script is developed to compute region-wise scaling ratios between the simulated and clinical reconstructions, and to generate a new activity map accordingly. First, the xAAL atlas registered to the reconstruction space is used to extract anatomical regions of interest. For each labeled region, the mean intensity is computed separately in the clinical and simulated images. A ratio is calculated as the quotient of clinical to simulated mean intensity *(see Equation 3)* and stored in a ratio map with the same spatial dimensions as the atlas.

$$ratio = \frac{mean_{clinical}}{mean_{simulated}} \quad \text{(Equation 3)}$$

These ratios are also exported to an Excel table for further inspection. To improve interpretability, the script then enriches the Excel book with anatomical region names by merging it with the reference file containing xAAL label definitions. Although this ratio map is resampled to simulation resolution by means of a nearest neighbout interpolation, the designed approach does not consist on directly multiplying this ratio map to the activity map for scale it. Resampling from the reconstruction resolution to simulation space is basically doing the inverse process we did when going from simulation to reconstruction space. However, simulation space has much more resolution than reconstruction one, therefore, the resampling from a lower resolution space to a

higher one could lead to inaccuracies and undesired changes in the ratios values. Because of this, ratios for each region are extracted from the saved Excel file and copied to the atlas resampled to simulation space according to the label each voxel belongs to. This way, the ratios values used to modify the activity map have not suffered any resampling process that could have altered them.

The script generates a new activity map by scaling the previous one in each iteration. Regions without a valid ratio (not represented in the atlas filled with ratios) are filled with the mean ratio computed from occipital regions, which are assumed to represent the reference activity. This step is crucial to maintain the magnitude and scale of the regions or voxels that are not included in the atlas used to adjust. Despite these regions not being taken into account for the comparison with clinical SPECT, this way we ensure that all voxels in the image are rescaled along with the brain to preserve all the activities as relative (proportional to the one in the occipital), even the activity of extracellular components.

The resulting product is normalized and scaled to an 8-bit intensity range (0–127) to comply with the input format required by the simulation software. Finally, the updated activity map is saved in both NIfTI and Analyze formats, ready to be passed to the next iteration of the simulation pipeline. This entire process ensures that each iteration reflects targeted, region-specific improvements in similarity between simulated and clinical images.

The described workflow is schematically represented in *Figure 24*.

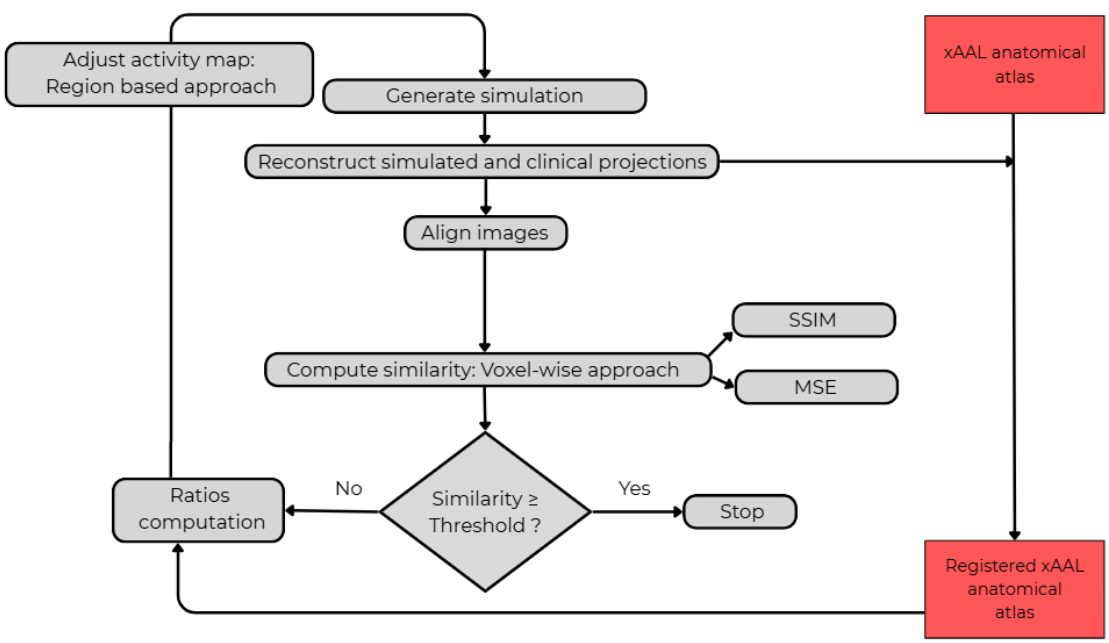

Figure 24. Schematic of the designed iterative framework (Own source)

5.5.1. Stopping criteria

In the design of the pipeline, the stopping criterion for the proposed iterative process was defined through a combined evaluation using both SSIM and MSE metrics, as this dual approach provides a more comprehensive assessment of similarity. While SSIM captures structural and perceptual

resemblance between the clinical and simulated images, MSE quantifies the voxel-wise intensity differences, offering complementary insights. The initial proposals were: a threshold of SSIM ≥ 0.8 to ensure sufficient structural similarity, alongside a Mean Squared Error (MSE) ≤ 0.005, which is understood as a reasonable limit indicating acceptable numerical agreement. This combined criterion ensures that the iterative adjustments yield reconstructions that are not only visually consistent with clinical data but also quantitatively accurate, providing a robust and balanced foundation for convergence.

5.6.Results and Discussion

When testing the iterative process on the subjects from the dataset, the results confirmed the following: in general, the similarity between the clinical and simulated reconstructions increases with each iteration. However, a few subjects were excluded from the evaluation due to failures in the realignment step between clinical and simulated reconstructions. This step is critical for ensuring that SSIM and MSE are accurately calculated, and any misalignment would compromise the validity of these metrics.

One notable observation is that the activity map tends to undergo substantial adjustments during the first iteration, but subsequent iterations result in much smaller changes. This indicates that the magnitude of adjustment needed progressively decreases, as the difference (or ratio) between simulated and clinical region intensities becomes smaller with each cycle.

In *Figure 25*, an example is shown illustrating how the activity map evolves over two iterations (in addition to the initial simulation) for a single subject, along with the corresponding reconstructions generated from each cycle, compared to the clinical reconstruction.

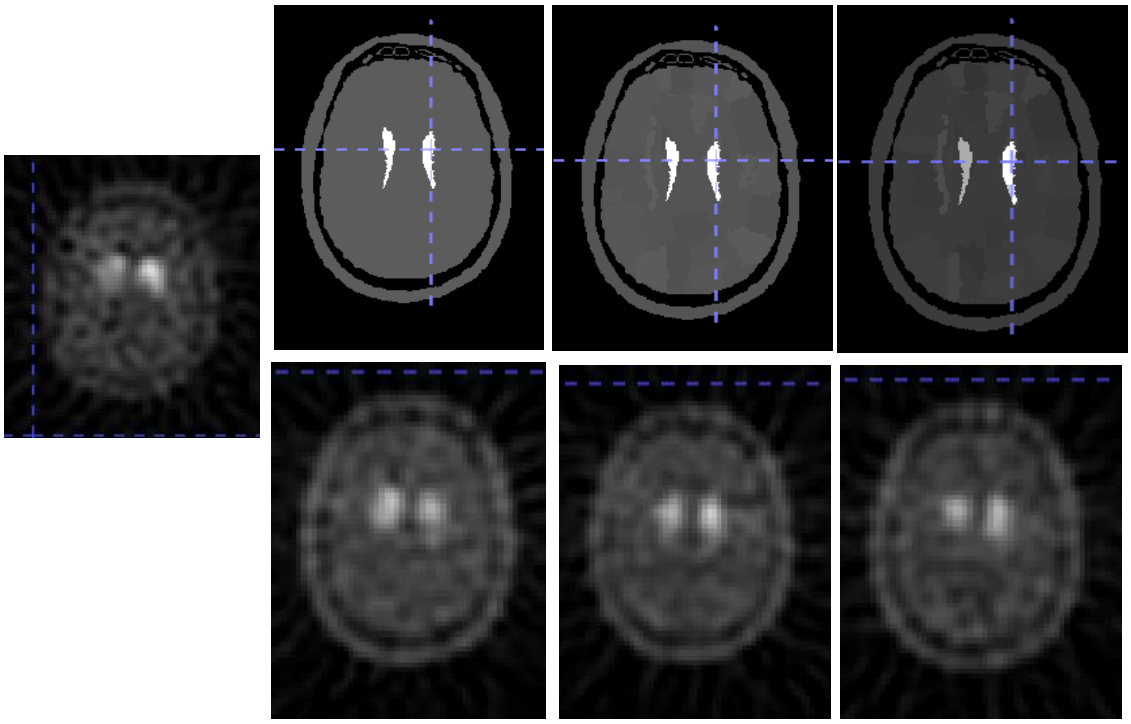

Figure 25. Evolution of the activity map and the simulated images over 2 iterations (First column corresponds to the original simulation and left image to the clinical reconstruction) (Own source)

It is worth noting that when the initial iteration already achieves a high similarity score, as happens with the subject shown above *(see Figure 25)* the improvements in subsequent iterations are minimal and often negligible.

For most subjects, realism improves progressively with each iteration but eventually reaches a plateau. In some cases, minor oscillations in similarity scores are observed, which may even result in slight decreases in SSIM or increases in MSE. Results for 3 patients are displayed in *Figures 26 and 27*. This suggests that the framework reaches a point where further updates do not improve and can oscillate and even provide worse returns.

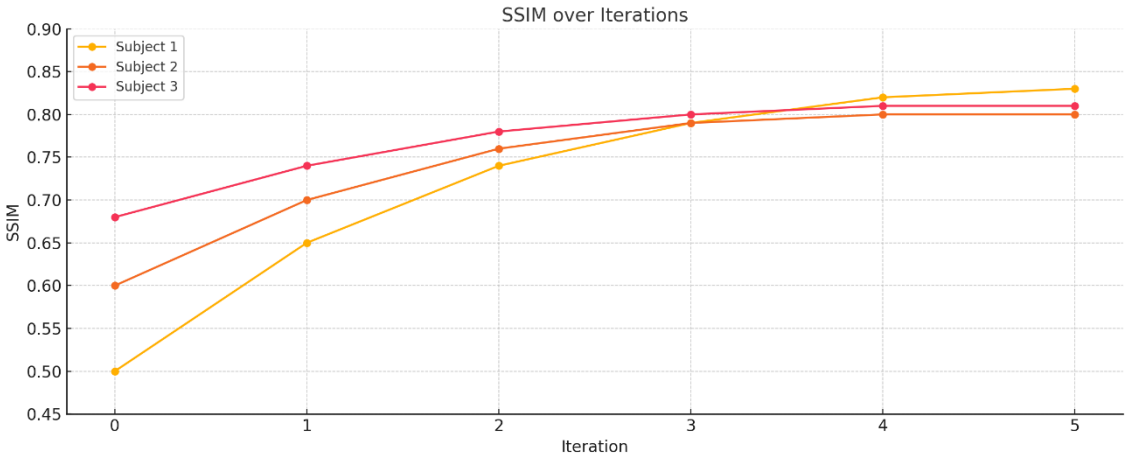

Figure 26. Evolution of SSIM values across iterations for three representative subjects. (Own source)

This plot shows how the **Structural Similarity Index (SSIM)** evolves over the iterations for three different subjects. Each line represents a subject and starts from a different initial similarity level, reflecting inter-subject variability. In all cases, the SSIM improves progressively across iterations, indicating that the iterative adjustments are effectively increasing the structural similarity between simulated and clinical reconstructions. The curves tend to stabilize in later iterations, suggesting convergence of the process.

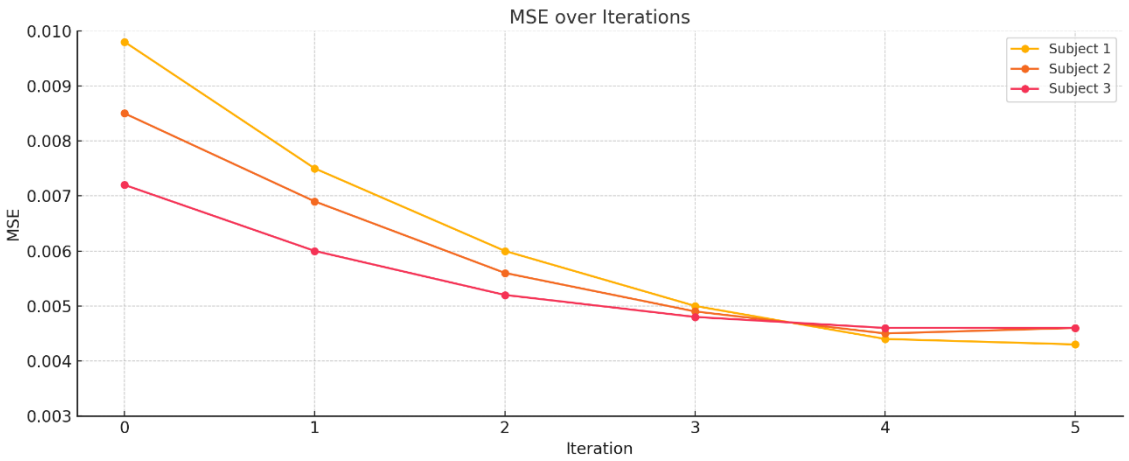

Figure 27. Evolution of MSE values across iterations for the same subjects. (Own source)

This plot illustrates the evolution of the **Mean Squared Error (MSE)** between simulated and clinical reconstructions for the same three subjects. Lower MSE values indicate higher numerical similarity. All subjects exhibit a consistent reduction in MSE through the iterations, with a sharp improvement in the early steps followed by stabilization. The decreasing trend confirms that the activity map adjustments are reducing voxel-wise intensity differences, complementing the SSIM analysis.

SSIM and MSE reflect very different aspects of similarity. As such, in some of the subjects tested, improvements in one metric do not always correspond to improvements in the other. This reinforces the idea of either using both measures jointly to evaluate convergence or studying a more suitable metric.

Finally, based on the observed behavior, it is proposed that the stopping criterion should not rely on a fixed threshold, but rather on convergence. Specifically, the process should stop when both SSIM and MSE stabilize, i.e., when neither shows significant improvement compared to previous iterations. This adaptive criterion would make the framework more robust and generalizable across different subjects.

6. Execution schedule

In this section one of the crucial parts of the planification of a project is represented: the expected temporal distribution. Usually, time is one of the limiting factors of the projects, as in our case, so it is of high importance to correctly split the tasks and assign them a reasonable amount of time.

6.1. Work Breakdown Structure (WBS)

This section focuses on outlining the various tasks required to successfully complete the project. *(Figure 28)*

WBS Chart

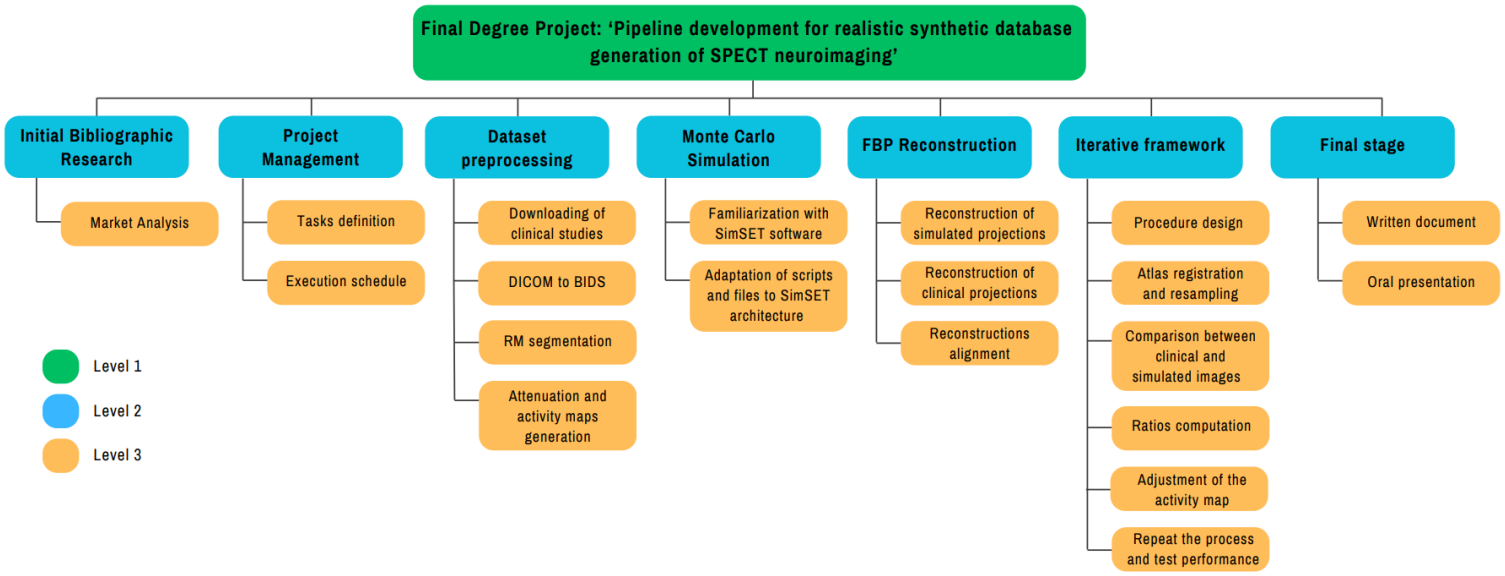

Figure 28. WBS Chart (Own source)

WBS Dictionary

Code	Task name	Description	Duration
1	INITIAL BIBLIOGRAPHIC RESEARCH		
1.1	Market Analysis	Literature review on SPECT simulation softwares and iterative projects such as BrainViset.	3 days
2	PROJECT MANAGEMENT		
2.1	Tasks definition	Definition of the objectives and the methodology to accomplish them. Division of the procedure into tasks.	2 days
2.2	Execution Schedule	Planning of the Project timming.	1 day
3	DATASET PREPROCESSING		
3.1	Downloading of clinical studies	Dataset generation from the hospital repository.	3 days
3.2	DICOM to BIDS	Images are converted to NIfTI format and organized following BIDS architecture.	4 days
3.3	RM segmentation	Generation of anatomical masks using MR images and FSL tools.	15 days
3.4	Attenuation and activity maps generation	Development a Python script to create attenuation and activity maps.	10 days
3	MONTE CARLO SIMULATION		
3.1	Familiarization with SimSET Software	Launch first simulations and analyze the configuration setup of SimSET.	7 days
3.2	Adaptation of scripts and files to SimSET architecture	Adapt the maps generation code to match with the simulator expected inputs and launch noisy simulations.	8 days
4	FBP RECONSTRUCTION		
4.1	Reconstruction of simulated projections	Python-based FBP pipeline applied to simulated projections.	7 days
4.2	Reconstruction of clinical projections	FBP reconstruction of real SPECT images by means of Windows executables.	4 days
4.3	Reconstrutions alignment	Transformation of clinical reconstruction to simulated MRI patient space.	3 days
5	ITERATIVE FRAMEWORK		
5.1	Procedure design	Study of the possible solutions to approach the iterative pipeline.	4 days

5.2	Atlas Registration and Resampling	Transforming xAAL atlas to patient space and resampling it to both simulation and reconstruction resolutions.	4 days
5.3	Comparison between clinical and simulated images	Computation of SSIM and MSE within the brain mask.	5 days
5.3	Ratios Computation	Regional mean intensity comparison and ratio map creation.	4 days
5.4	Adjustment of the activity map	Generation of new activity map based on correction ratios.	3 days
5.5	Repeat process and test performance	Execution of next simulation iterations and tracking results.	10 days
6	FINAL STAGE		
6.1	Written document	Throughout the execution of the project, a memory of the process performed is written.	40 days Deliverable: 11/06/2025
6.2	Oral presentation	Slide creation and rehearsal for defense. (10 minutes)	5 days Deliverable: 19/06/2025

Table 1. WBS dictionary (Own source)

6.2.Precedence analysis and critical path method

To estimate the duration (in days) required for each task, a precedence analysis has been performed. The expected time for each task is calculated using the **PERT (Program Evaluation and Review Technique)** method.

Task	ID	Preceding activities	Duration (days)	Looseness (days)
1.1 Market Analysis	A	-	3	76
2.1 Tasks definition	B	-	2	1
2.2 Execution schedule	C	B	1	76
3.1 Downloading of clinical studies	D	-	3	0
3.2 DICOM to BIDS	E	B, D	4	0
3.3 RM segmentation	F	E	15	0
3.4 Attenuation and activity maps generation	G	F	10	0
4.1 Familiarization with SimSET software	H	G	7	0

4.2 Adaptation of scripts and files to SimSET architecture	I	H	8	0
5.1 Reconstruction of simulated projections	J	I	7	0
5.2 Reconstruction of clinical projections	K	E	4	43
5.3 Reconstructions alignment	L	J, K	3	0
6.1 Procedure design	M	B	4	51
6.2 Atlas registration and resampling	O	G	4	43
6.3 Comparison between clinical and simulated images	N	L, M	5	0
6.4 Ratios computation	P	M, K, O	4	0
6.5 Adjustment of the activity map	Q	M, P	3	0
6.6 Repeat the process and test performance	R	Q	10	0
7.1 Written document	S	-	40	34
7.2 Oral presentation	T	S	5	34

Table 2. Data for precedence analysis (Own source)

The activities with no looseness make up the **critical path**.

6.3.GANTT Chart

Project conducted from February to June, one meeting per week with director and tutor of the project. Timing of the project displayed in *Figure 29.*

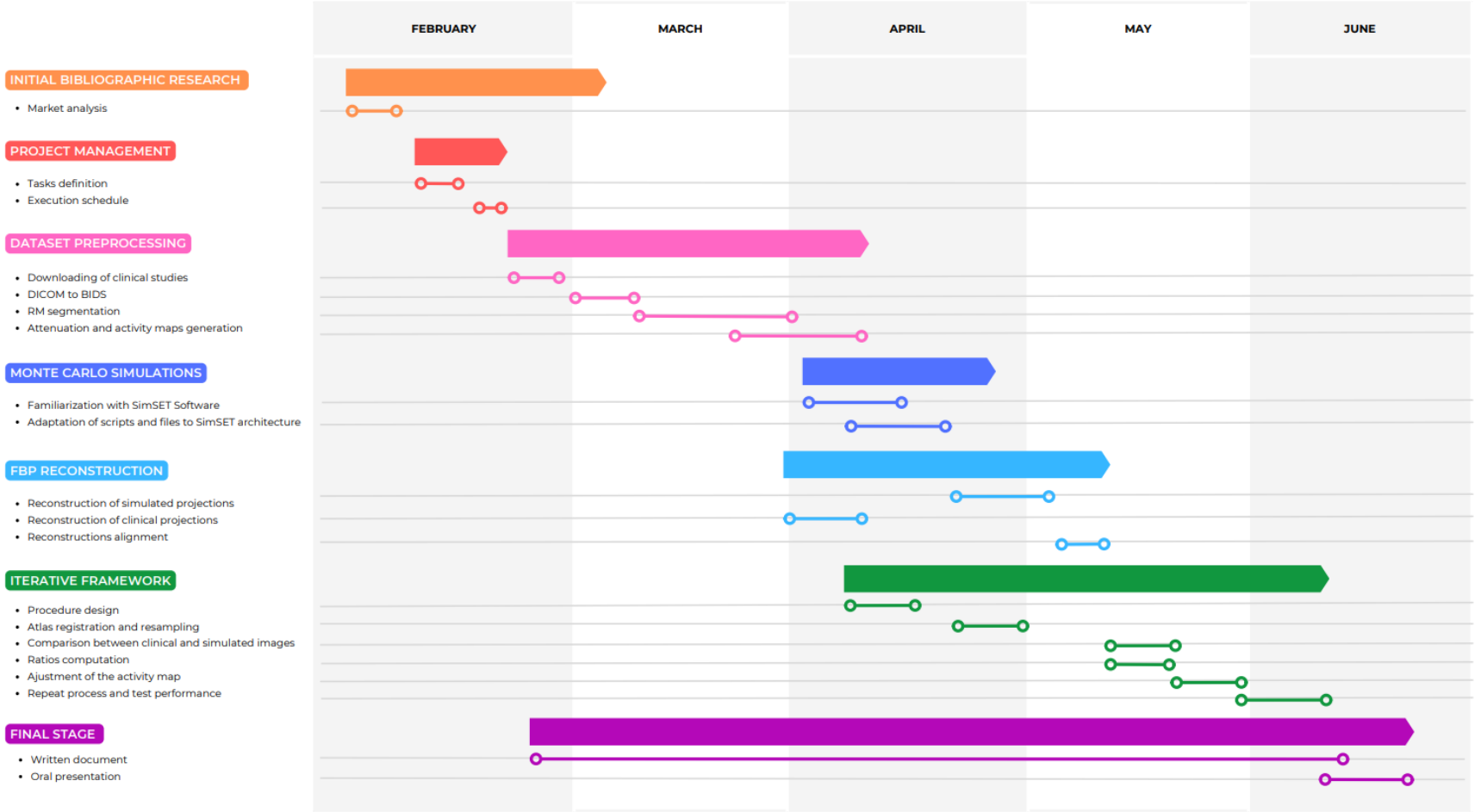

Figure 29. GANTT diagram of the project (Own source)

7. Technical feasibility

7.1.SWOT Analysis

In this section, a technical viability study will be conducted using the SWOT analysis method, which involves listing the project's strengths and weaknesses (internal origin) but also its opportunities and threats (external origin). This approach provides an overall assessment of the project's feasibility and highlights potential challenges that may arise during the development of the chosen solution. The SWOT diagram is illustrated in Figure XX.

Figure 30. SWOT matrix (Own source)

While most points in the matrix are self-explanatory, it is worth clarifying that the lack of realistic noise modeling in SimSET refers to the fact that simulation parameters are not explicitly tuned to match the noise characteristics of real clinical acquisitions, which limits absolute realism. Regarding weaknesses such as “remote work and availability of cluster resources,” these point to the shared nature of the SOL computing infrastructure, where node usage may be restricted or delayed depending on other users’ activity. Similarly, “operating system dependency” in the threats section refers to the division of workflows between Linux (with Ubuntu operating system) and Windows environments, which may complicate portability or future integration. Moreover, since working with real data, the project must comply with data privacy regulations, which are specified in section 9 (Legal aspects). Finally, the “temporal limitation of the project” reflects the constraints of a time-

bounded academic setting, which limits the exploration of more complex or long-term developments.

Among all the aspects mentioned above, experience and abilities of the user have to be analyzed as well. Here, we focus on programming knowledge and prior experience dealing with imaging datasets and Ubuntu operating system, since this skills are crucial for the development of the pipeline. In this case, previous knowledge on imaging and programming was acquired in courses like 'Biomedical Imaging Computing Laboratory', 'Computer science' and 'Biomedical Imaging'.

Taking all of this into account, we can expect that the strengths of the project will help overcoming its weaknesses, and although there might be some threats, the potential opportunities in having success on the project have more weight. Consequently, we can consider that the project is feasible and possible to execute in the terms it has been raised.

7.2. Technical specifications

The project has been developed using a combination of specialized software tools, programming libraries, and computing infrastructure tailored to neuroimaging research and Monte Carlo simulation. All tools used are either open-source, available for academic use, or were provided through the technical environment of the research group where the project was conducted.

For image preprocessing and segmentation, key tools include **FSL** (FMRIB Software Library), used for brain extraction, bias correction, and registration tasks, and **ANTs** (Advanced Normalization Tools), which provide state-of-the-art rigid, affine, and non-linear registration capabilities. Both FSL and ANTs are free for academic use and were pre-installed on the laboratory systems.

SimSET (Simulation System for Emission Tomography) is the core simulation engine employed and is freely available for non-commercial academic purposes. All simulations are launched by means of bash scripts.

For visualization, the project relies on **ITK-SNAP**, a free and open-source application designed for medical image navigation and annotation. This tool has also been useful for validating registration accuracy and inspecting image quality throughout the processing pipeline.

The programming language used for most of the scripts is **Python**, with the majority of development done using the **Spyder IDE**, which provides an integrated development environment suited for scientific computing. A custom Python virtual environment was configured to include all required packages:

- nibabel: for handling NIfTI and Analyze image formats
- numpy and pandas: for data manipulation and numerical analysis
- skimage: for filters and SSIM computation
- matplotlib: for visualization
- ANTsPy: for applying spatial transforms and resampling

For remotely accessing the Linux simulation server from a Windows workstation, **WinSCP** was used to manage secure file transfers and remote directory navigation.

To enable image conversion and reconstruction, the project used several dedicated **executables**, including *dcm2nii* for DICOM-to-NIfTI conversion and tools like *fbpreconstruction* and *buttFilter* for SPECT image reconstruction. These executables were either provided by the research laboratory or downloaded from free-access resources.

This set of tools, combined with modular code design and a consistent file structure, ensured technical feasibility, reproducibility, and scalability throughout the project.

8. Economic viability

From an economic perspective, the implementation of this project is highly feasible. To evaluate it in more detail, a breakdown of costs into key categories is displayed: personnel, material, computing, and indirect expenses.

On the one hand we must consider the human resources costs of the author of this project but also her advisors. Total hours are defined in accordance with the stipulated in the Final Degree Project guidelines is assumed: 300 hours for the student and 80 hours for the tutors. The salary data is an estimation because in the real context, as it is a Final Degree project, there has not been any financial compensation for the engineering student.

Concept	***Salary***	***Total cost***
Sara Álvarez Gamero (Student)	7 €/h	2100 €
Aida Niñerola Baizán (Senior Engineer)	20 €/h	1600€
Raúl Tudela Fernández (Senior Engineer)	20 €/h	1600€
Total Human Resources cost		**5300 €**

Table 3. Human resources of the project (Own source)

On the other hand, we have to consider the material resources employed:

Concept	***Unitary cost***	***Total cost***
Personal computer	600 €	600 €
Department computer	1500 €	1500 €
Total Material Resources cost		**2100 €**

Table 4. Material resources of the project (Own source)

Also, a consideration of all software tools and licenses used in this project is done. In the list, the software packages used appear:

Concept	Unitary cost	Total cost
WinSCP	Free software (0€)	0€
SimSET	Free software (0€)	0€
Spyder IDE	Free software (0€)	0€
ITK-SNAP	Free software (0€)	0€
Office 365 license	5,60€/month	28€ (5 months)
Total Computing Resources cost		**28 €**

Table 5. Computing resources of the project (Own source)

Finally, we also have to consider our stay at the lab and the work at home, and the associated costs it brought during these months in terms of energy. This is the distribution of costs assuming that we worked 4 days/week, at the laboratory from February to May and from home in May and June. Total expense is an estimation.

Concept	Unitary cost	Total cost
Electricity costs	0.50€/day	40 €
Laboratory consumption	30€/day	1500 €
Total Indirect cost		**1,540 €**

Table 6. Indirect cost of the project (Own source)

Considering all expenses, the total estimated budget of the project is: **8.968€**

To complement this, the following pie chart shows the percentage allocation of resources across cost categories:

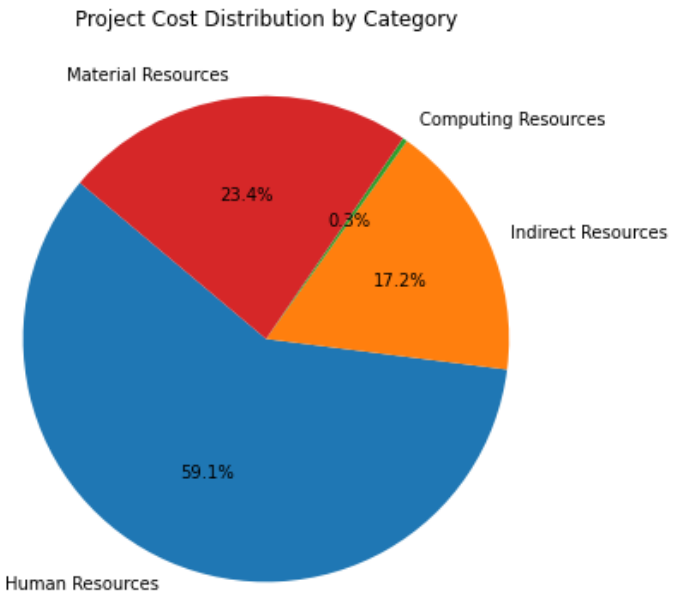

Figure 31. Pie chart of the project's cost distribution (Own source)

This cost-effective design makes the proposed methodology suitable not only for academic research but also for future clinical software validation processes. Furthermore, the scalability of the pipeline enables future extensions, such as the generation of large synthetic image datasets or integration into regulatory-grade validation tools, without significant additional financial burden.

9. Legal aspects

In general, all Final Degree Projects at the University of Barcelona must comply with the institution's **Code of Research Integrity**. This code is based on key values such as honesty, responsibility, reliability, rigor, respect, and independence, and applies to all academic and research personnel. It establishes the foundations of intellectual authorship and explicitly condemns any form of academic misconduct, including plagiarism, data falsification, and fabrication. [70]

The current project operates entirely in a research context and involves only anonymized clinical image data with no direct involvement of patients or personal health information. Therefore, it complies with **GDPR (General Data Protection Regulation)** and does not require specific ethical approval. All image datasets are previously acquired under existing clinical protocols and anonymized before use. [71]

Regarding the potential applicability of this pipeline, regulatory bodies are responsible for certifying the clinical safety and performance of diagnostic tools. Agencies such as the U.S. **Food and Drug Administration (FDA)** are actively encouraging the use of simulation and computational modeling in medical device evaluation. The FDA's framework for modeling credibility highlights the role of simulation in preclinical assessment and risk evaluation of imaging systems (FDA, 2023). The regulatory sector is not treated as a target market for the project because these agencies rarely conduct validations themselves; instead, they require robust evidence from developers, for which simulated datasets can serve as a standardized, reproducible foundation. [72]

Similarly, in the European context, **CE marking** under the **Medical Device Regulation** (EU MDR 2017/745) also demands strong technical documentation demonstrating performance and safety. Simulated data can be used to support software verification and validation, especially for higher-risk classes where conformity assessments by notified bodies are mandatory. This makes high-fidelity synthetic datasets a valuable asset in streamlining regulatory submissions and accelerating product approval. The use of simulation to generate known ground-truth data contributes directly to the technical validation step required in CE marking processes. Projects such as BrainViSet have demonstrated that synthetic data can serve as a valuable tool for early-stage software evaluation, fulfilling part of the "clinical evidence" requirement in MDR [54]. [73]

The project itself aligns with the European Medical Device Regulation (EU MDR 2017/745) in spirit, as its long-term goal is to contribute to the development and validation of medical image quantification software. According to MDR guidelines, software intended for diagnostic or therapeutic purposes is considered a medical device and must be validated using reliable datasets. Therefore, in the future, any translation of this pipeline into clinical applications or commercial tools

would require formal certification and clinical trials. However, at its current stage, the project is compliant with research best practices and serves as a foundational step for regulatory-compliant software development in nuclear medicine.

10. Conclusions and future lines

10.1. General conclusions

In this project, a pipeline has been successfully developed to iteratively generate realistic SPECT images from anatomical data. The proposed methodology has been tested using real patient datasets, with the results suggesting its capability to refine simulated activity maps and improve similarity with clinical reconstructions over multiple iterations.

The pipeline has been specifically adapted to the SimSET simulation architecture and includes integrated quality control steps throughout the image processing workflow. Preprocessing scripts and map generation modules have been optimized to support execution for large cohorts, significantly improving scalability and usability.

One of the critical challenges encountered during the project was the segmentation of MR images. In particular, the performance of FSL BET proved to be more limited than expected, resulting in the exclusion of several subjects due to inaccurate brain extractions. This highlights the importance of robust and adaptable segmentation tools when designing automated pipelines for neuroimaging applications.

While both clinical and simulated projections were reconstructed using the same algorithm (FBP), the reconstruction script itself is not yet fully generalizable across both data types, which may limit its portability to other datasets or clinical environments.

Regarding the evaluation of similarity, the project used SSIM and MSE as reference metrics. Although these provide complementary perspectives (structural and intensity-based respectively),it remains unclear whether they are the most appropriate indicators for comparing simulated and clinical reconstructions. In some cases, the two metrics yielded conflicting results, suggesting that further study is needed to validate or refine these measures for this specific context.

Based on the results obtained, the project proposes a convergence-based stopping criterion: the iterative process should terminate when both SSIM and MSE stabilize across consecutive iterations. However, to confirm the robustness and general applicability of this criterion, future work should test it on larger and more diverse datasets.

Overall, this work lays the groundwork for realistic SPECT simulation using patient-specific anatomical information and contributes a flexible, extensible framework that can be further improved and adapted to future clinical and research applications.

10.2. Future work

As further work is expected for this project, all the scripts involved in the project and a set of guidelines have been provided to the director to ease the future adaptation and implementation of the developed pipeline.

There are several potential avenues to further develop and enhance the framework established in this project. One of the most immediate and impactful next steps would be the **full automation of the entire pipeline**, from initial data input to the final similarity evaluation and map adjustment. While the current implementation integrates a high degree of automation, some stages still require manual supervision. Streamlining the entire process into a single, user-independent workflow would not only reduce the risk of human error but also enable large-scale testing across extended datasets with minimal intervention.

Another promising direction would be to explore an **alternative adjustment strategy based on voxel-wise corrections**, rather than the current region-based approach. In the present framework, activity scaling is performed uniformly within predefined anatomical regions extracted from the xAAL atlas. While this method is efficient and interpretable, it may limit spatial precision and overlook subtle, localized discrepancies between clinical and simulated images. A voxel-level adjustment, on the other hand, could allow for **finer granularity**, potentially capturing microstructural differences and heterogeneity that are not represented at the regional level. This approach could also remove the dependency on atlas registration and labeling quality, which sometimes introduces uncertainty into the adjustment process. Implementing and validating voxel-based scaling, however, would require careful regularization strategies to avoid overfitting local noise and to preserve physiological plausibility in the resulting activity maps.

Regarding the ultimate intention of this project: The integration of realistic SPECT simulation studies to validate acquisition, reconstruction, or quantification methods is complex, requiring scripting knowledge to execute the processes. In the event that this project is improved in the future and actually ends up giving rise to a database of realistic simulated SPECT images intended to be used to validate quantification methods; the theoretical SUR value (obtained from the activity map that generated the last simulated iteration) must be computed and provided to the user for each of the images. It can be calculated using the masks generated from the segmentation of striatal regions and the last activity map which generated the final simulation iteration. This theoretical SUR value should be used as ground truth by comparing it to the SUR value the quantification method obtains from quantifying the reconstruction image in question.

11. Bibliography

[1] National Institute on Aging. (2022). *Parkinson's disease: Causes, symptoms, and treatments*. https://www.nia.nih.gov/health/parkinsons-disease

[2] NHS. (2022, November 11). *Causes of Parkinson's disease*. https://www.nhs.uk/conditions/parkinsons-disease/causes/

[3] Haider, A., Elghazawy, N. H., Dawoud, A., & et al. (2023). Translational molecular imaging and drug development in Parkinson's disease. *Molecular Neurodegeneration, 18*(11). https://doi.org/10.1186/s13024-023-00600-z

[4] Kangasmaa, T., Hippeläinen, E., Constable, C., et al. (2021). Quantitative Monte Carlo-based brain dopamine transporter SPECT imaging. *Annals of Nuclear Medicine, 35*, 17–23.

[5] Fang, Y.-H. D., Chiu, S.-C., Lu, C.-S., Yen, T.-C., & Weng, Y.-H. (s.f.). Fully automated quantification of the striatal uptake ratio of [99mTc]-TRODAT with SPECT imaging: Evaluation of the diagnostic performance in Parkinson's disease and the temporal regression of striatal tracer uptake. *BioMedical Research*.

[6] Booij, J., Dubroff, J., Pryma, D., Yu, J., Agarwal, R., Lakhani, P., & Kuo, P. H. (2017). Diagnostic performance of the visual reading of 123I-ioflupane SPECT images with or without quantification in patients with movement disorders or dementia. *Journal of Nuclear Medicine, 58*(11), 1821–1827.

[7] University of Washington. (n.d.). *SimSET: Simulation System for Emission Tomography*. Retrieved June 10, 2025, from https://depts.washington.edu/simset/html/simset_main.html

[8] Metropolis, N., & Ulam, S. (1949). The Monte Carlo method. Journal of the American Statistical Association, 44(247), 335–341. https://doi.org/10.1080/01621459.1949.10483310

[9] Jankovic, J. (2008). Parkinson's disease: Clinical features and diagnosis. *Journal of Neurology, Neurosurgery & Psychiatry, 79*, 368–376.

[10] Samii, A., Nutt, J. G., & Ransom, B. R. (2004). Parkinson's disease. *The Lancet, 363*(9423), 1783–1793.

[11] J. Jankovic y E. Tolosa, Parkinson's Disease and Movement Disorders, Lippincott Williams & Wilkins., 2007.

[12] Schapira, A. H., & Jenner, P. (2011). Etiology and pathogenesis of Parkinson's disease. *Movement Disorders, 26*(6), 1049–1055.

[13] Dauer, W., & Przedborski, S. (2003). Parkinson's disease: Mechanisms and models. *Neuron, 39*(6), 889–909.

[14] Hattori, N., & Mizuno, Y. (2004). Pathogenetic mechanisms of parkin in Parkinson's disease. *The Lancet, 364*(9435), 722–724.

[15] Barone, P. (2010). Neurotransmission in Parkinson's disease: Beyond dopamine. *European Journal of Neurology, 17*(3), 364–376.

[16] Blandini, F., Nappi, G., Tassorelli, C., & Marignoni, E. (1999). Functional changes of the basal ganglia circuitry in Parkinson's disease. *Progress in Neurobiology, 62*(1), 63–88.

[17] Wichmann, T., & DeLong, M. (2007). Anatomy and physiology of the basal ganglia: Relevance to Parkinson's disease and related disorders. In *Handbook of Clinical Neurology* (Vol. 83, pp. 1–18). Elsevier.

[18] Waxman, S. G. (2017). *Chapter 4: Abnormalities of movement and posture caused by disease of the basal ganglia*. In Clinical Neuroanatomy (27th ed.). McGraw-Hill Education. Retrieved from https://neupsykey.com/chapter-4-abnormalities-of-movement-and-posture-caused-by-disease-of-the-basal-ganglia/

[19] Nutt, J., Carter, J., & Sexton, G. (2004). The dopamine transporter: Importance in Parkinson's disease. *Annals of Neurology, 55*(6), 766–773.

[20] Tolosa, E., Wenning, G., & Poewe, W. (2006). The diagnosis of Parkinson's disease. *The Lancet Neurology, 5*(1), 75–86. https://doi.org/10.1016/S1474-4422(05)70285-4

[21] Jankovic, J., Rajput, A. H., McDermott, M. P., & Perl, D. P. (2000). The evolution of diagnosis in early Parkinson's disease. *Archives of Neurology, 57*(3), 369–372. https://doi.org/10.1001/archneur.57.3.369

[22] Ramaker, C., Marinus, J., Stiggelbout, A. M., & Van Hilten, B. J. (2002). Systematic evaluation of rating scales for impairment and disability in Parkinson's disease. *Movement Disorders, 17*(5), 867–876. https://doi.org/10.1002/mds.10248

[23] Goetz, C. G., Poewe, W., Rascol, O., Sampaio, C., Stebbins, G. T., Counsell, C., ... & Seidl, L. (2004). Movement Disorder Society Task Force report on the Hoehn and Yahr staging scale: Status and recommendations. *Movement Disorders, 19*(9), 1020–1028. https://doi.org/10.1002/mds.20213

[24] Niñerola-Baizán, A. (2015). *Quantification of striatal dopamine transporter SPECT in animal models and clinical research* [Doctoral dissertation, Universitat de Barcelona]. Unitat de Biofísica i Bioenginyeria.

[25] Yandrapalli, S. (2022, October 3). SPECT imaging. In *StatPearls*. StatPearls Publishing. https://www.ncbi.nlm.nih.gov/books/NBK564426/

[26] Martín-Comín, J., et al. (2012). *Medicina nuclear en la práctica clínica* (2ª ed., pp. 59–83). Aula Médica.

[27] European Medicines Agency. (2022, February 10). DaTSCAN. https://www.ema.europa.eu/en/medicines/human/EPAR/datscan

[28] Parkinson's Foundation. (s. f.). *Normal vs Parkinsonian DaTscan images* [Dopamine transporter SPECT images]. Parkinson's Foundation.

[29] Mayo Clinic. (2022, July 27). SPECT scan. https://www.mayoclinic.org/tests-procedures/spectscan/about/pac-20384925

[30] Themes, U. (2016, February 26). Tomographic reconstruction in nuclear medicine. In *Radiology Key*. https://radiologykey.com/tomographic-reconstruction-in-nuclear-medicine/

[31] Scirp.org. https://www.scirp.org/journal/paperinformation?paperid=27659

[32] Peters, S. M. B., van der Werf, N. R., Segbers, M., van Velden, F. H. P., Wierts, R., Blokland, K. J. A., … Gotthardt, M. (2019). *Towards standardization of absolute SPECT/CT quantification: A multi-center and multi-vendor phantom study*. EJNMMI Physics, 6, 29. https://doi.org/10.1186/s40658-019-0268-5

[33] Crespo, C., Gallego, J., Cot, A., Falcón, C., Bullich, S., & others. (2008). Quantification of dopaminergic neurotransmission SPECT studies with ^{123}I-labelled radioligands: A comparison between different imaging systems and data acquisition protocols using Monte Carlo simulation. *European Journal of Nuclear Medicine and Molecular Imaging, 35*(7), 1334–1342.

[34] Manohar, S., Sechopoulos, I., Anastasio, M. A., Maier-Hein, L., Gupta, R., & et al. (2023). Super phantoms: Advanced models for testing medical imaging technologies. *Nature Communications, 14*, 1234.

[35] Gong, K., Guan, J., Kim, K., Liu, C. C., Qi, J., & Liu, J. (2021). PET Image Denoising Using a Deep Neural Network Through Fine Tuning. *IEEE Transactions on Radiation and Plasma Medical Sciences, 5*(3), 364–373.

[36] SIMCor Project. (n.d.). *Simulation of Cardiac and Cardiovascular Devices for Regulatory Approval*. European Commission - CORDIS. Retrieved April 21, 2024, from https://cordis.europa.eu/project/id/101017578

[37] Paredes-Pacheco, J., Orts, J., Marti-Bonmati, L., & Alberich-Bayarri, A. (2021). SimPET: A Monte Carlo-based PET dataset for the validation of quantification and registration methods. *Medical Physics, 48*(7), 3582–3593. https://doi.org/10.1002/mp.14894

[38] Cao, N., et al. (2010). Detection performance analysis for time-of-flight PET. Physics in medicine and biology, 55(22), 6931–6950. https://doi.org/10.1088/0031-9155/55/22/021

[39] Voximetry Inc. (n.d.). *Accelerated radiopharmaceutical therapy with accurate dosimetry.* Retrieved from https://voximetry.com

[40] Subtle Medical. (n.d.). *Subtle Medical – Enabling smarter, safer medical imaging.* Retrieved June 10, 2025, from https://subtlemedical.com/

[41] Mirada Medical. (2023). *AI-powered quantitative analysis software.* https://www.mirada-medical.com

[42] MIM Software. (n.d.). *Quantitative imaging solutions.* Retrieved from https://www.mimsoftware.com

[43] Hermes Medical Solutions. (2022). *Simulated data and AI for nuclear medicine quantification.* Retrieved from https://www.hermesmedical.com

[44] European Association of Nuclear Medicine. (n.d.). *EANM – European Association of Nuclear Medicine*. Retrieved June 10, 2025, from https://eanm.org/

[45] GE Healthcare. (n.d.). *DaTQUANT™ for quantitative analysis of DaTSCAN™ images*. from https://www.gehealthcare.com/products/molecular-imaging-agents/datquant.

[46] Gamma Gurus Pty Ltd. (n.d.). *Hoffman 3-D Brain Phantom*. https://gammagurus.com/products/hoffman-3-d-brain-phantom

[47] Radiology Support Devices, Inc. (n.d.). *Striatal Phantom*. from https://rsdphantoms.com/product/striatal-phantom/

[48] Los Alamos National Laboratory. (n.d.). *Monte Carlo N-Particle Transport Code System (MCNP)*. from https://mcnp.lanl.gov/

[49] OpenGATE Collaboration. (n.d.). *GATE documentation (v9.0)*. from https://opengate.readthedocs.io/en/v9.0/introduction.html

[50] Lund University. (n.d.). SIMIND Monte Carlo Program for SPECT. from https://simind.blogg.lu.se/

[51] STRATOS Initiative. (n.d.). Strengthening Analytical Thinking for Observational Studies. https://stratos-initiative.org/

[52] Paredes-Pacheco, J., López-González, F. J., Silva-Rodríguez, J., Efthimiou, N., Niñerola-Baizán, A., Ruibal, Á., Roé-Vellvé, N., & Aguiar, P. (2021). SimPET—An open online platform for the Monte Carlo simulation of realistic brain PET data. Validation for 18F-FDG scans. Medical Physics, 48(5), 2482-2493. https://doi.org/10.1002/mp.14838

[53] ASIM PET simulator. (s. f.). University of Washington.

[54] Marti-Fuster, B., Esteban, O., Thielemans, K., Setoain, X., Santos, A., Ros, D., & Pavia, J. (2014). Including Anatomical and Functional Information in MC Simulation of PET and SPECT Brain Studies. Brain-VISET: A Voxel-Based Iterative Method. IEEE Transactions On Medical Imaging, 33(10), 1931-1938. https://doi.org/10.1109/tmi.2014.2326041

[55] FSL - the FMRIB Software Library. (s. f.). https://fsl.fmrib.ox.ac.uk/fsl/docs/#/

[56] SPM - Statistical Parametric Mapping. (s. f.). Functional Imaging Laboratory © 2023. https://www.fil.ion.ucl.ac.uk/spm/

[57] FreeSurfer. (s. f.). FreeSurfer. https://surfer.nmr.mgh.harvard.edu/

[58] Nett, B., PhD. (2022, 27 abril). Filtered BackProjection (FBP) Illustrated Guide For Radiologic Technologists • How Radiology Works. How Radiology Works. https://howradiologyworks.com/filtered-backprojection-fbp-illustrated-guide-for-radiologic-technologists/

[59] Lantos, J., Mittra, E. S., Levin, C. S., & Iagaru, A. (2018). Standard OSEM vs. regularized PET image reconstruction: qualitative and quantitative comparison using phantom data and various clinical radiopharmaceuticals. American Journal of Nuclear Medicine and Molecular Imaging, 8(2), 110–118.

[60] Li, X., Morgan, P. S., Ashburner, J., Smith, J., & Rorden, C. (2016). The first step for neuroimaging data analysis: DICOM to NIfTI conversion. Journal of Neuroscience Methods, 264, 47–56.

[61] BIDS - the Brain Imaging Data Structure. (s. f.). https://bids.neuroimaging.io/index.html

[62] Mic-Dkfz. (s. f.). GitHub - MIC-DKFZ/HD-BET: MRI brain extraction tool. GitHub. https://github.com/MIC-DKFZ/HD-BET

[63] Introduction - BET. (s. f.). https://open.win.ox.ac.uk/pages/fslcourse/practicals/intro2/index.html

[64] FAST. (s. f.). https://web.mit.edu/fsl_v5.0.10/fsl/doc/wiki/FAST.html

[65] FIRST/UserGuide. (s. f.). https://web.mit.edu/fsl_v5.0.10/fsl/doc/wiki/FIRST(2f)UserGuide.html

[66] AAL atlas. (s. f.). Nilearn. https://nilearn.github.io/stable/modules/description/aal.html

[67] Contributors to Wikimedia projects. (2025, 2 marzo). Índex de similitud estructural. Viquipèdia, L'enciclopèdia Lliure. https://ca.wikipedia.org/wiki/%C3%8Dndex_de_similitud_estructural

[68] Registration — ANTsPy dev (latest) documentation. (s. f.). https://antspy.readthedocs.io/en/latest/registration.html

[69] Contributors to Wikimedia projects. (2025b, marzo 29). Error quadràtic mig. Viquipèdia, L'enciclopèdia Lliure. https://ca.wikipedia.org/wiki/Error_quadr%C3%A0tic_mig

[70] FAQ's | Bioethics Commission. (s. f.). https://www.ub.edu/comissiobioetica/en/faqs

[71] General Data Protection Regulation (GDPR) – legal text. (2024, 22 abril). General Data Protection Regulation (GDPR). https://gdpr-info.eu/

[73] Office of the Commissioner. (s. f.). *U.S. Food and Drug Administration*. U.S. Food And Drug Administration. https://www.fda.gov/

[74] *Regulation - 2017/745 - EN - Medical Device Regulation - EUR-LEX*. (s. f.). https://eur-lex.europa.eu/eli/reg/2017/745/oj/eng

12. Annexes

Annex 1

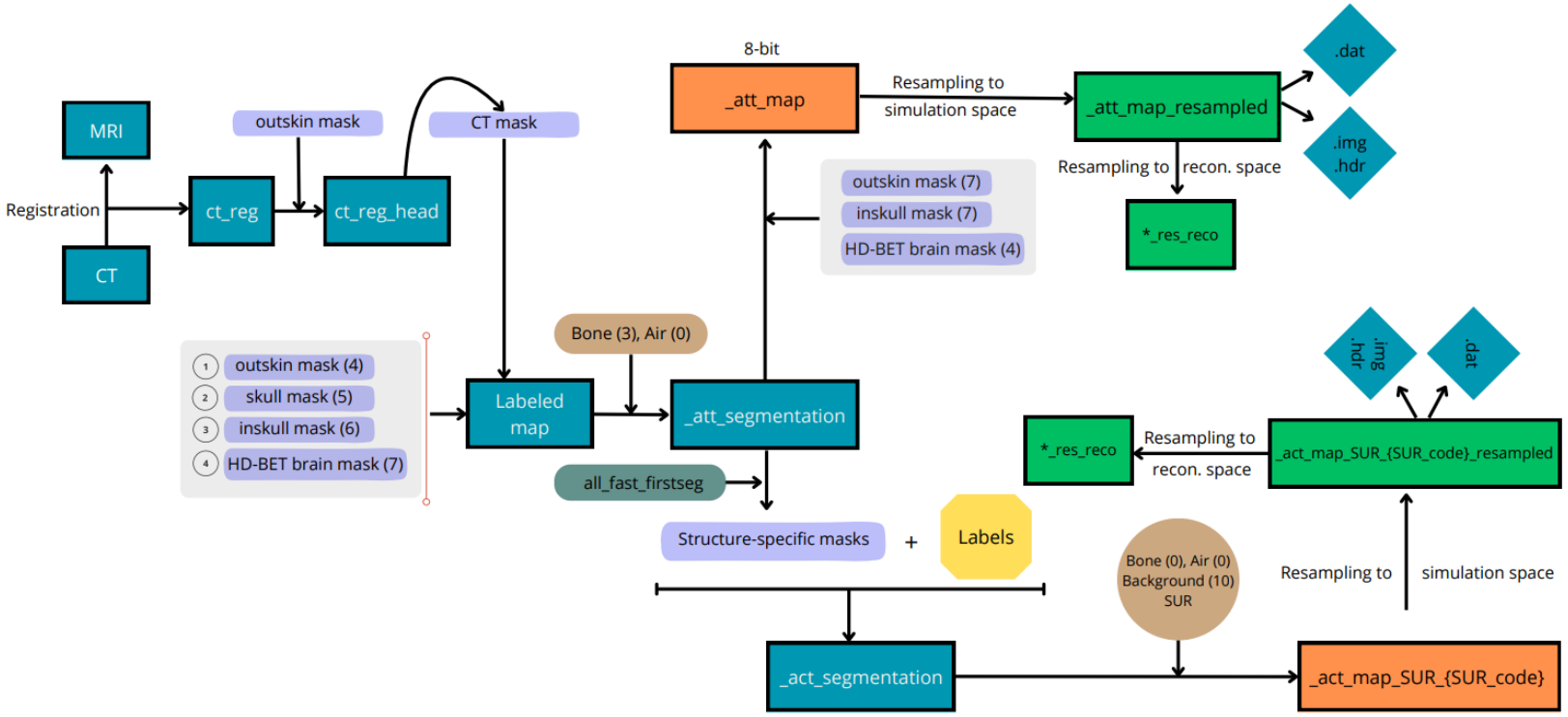

Figure A1. Summary of the attenuation and activity maps generation (Own source)